Remote Sensing of Environment 303 (2024) 114013

Contents lists available at ScienceDirect

Remote Sensing of Environment

journal homepage: www.elsevier.com/locate/rse

Towards a standardized, ground-based network of hyperspectral measurements: Combining time series from autonomous field spectrometers with Sentinel-2

Paul Naethe [a,*], Andrea De Sanctis [a], Andreas Burkart [a], Petya K.E. Campbell [b,c], Roberto Colombo [d], Biagio Di Mauro [e], Alexander Damm [f,g], Tarek El-Madany [h], Francesco Fava [i], John A. Gamon [j,k], Karl F. Huemmrich [b,c], Mirco Migliavacca [l], Eugenie Paul-Limoges [g,m], Uwe Rascher [n], Micol Rossini [d], Dirk Schüttemeyer [o], Giulia Tagliabue [d], Yongguang Zhang [p], Tommaso Julitta [a]

[a] JB Hyperspectral Devices GmbH, Am Botanischen Garten 33, 40225 Duesseldorf, Germany
[b] Joint Center for Earth Systems Technology (JCET), University of Maryland Baltimore County, Baltimore, MD 21228, USA
[c] Biospheric Sciences Laboratory, NASA Goddard Space and Flight Center, Greenbelt, MD 20771, USA
[d] Remote Sensing of Environmental Dynamics Lab., Dept. of Earth and Environmental Sciences, University of Milano-Bicocca, Piazza della Scienza 1, Milano 20126, Italy
[e] Institute of Polar Sciences, National Research Council, Via Cozzi 53, 20125 Milan, Italy
[f] EAWAG Swiss Federal Institute of Aquatic Science and Technology, Duebendorf, Switzerland
[g] Department of Geography, University of Zurich, Zurich, Switzerland
[h] Department Biogeochemical Integration, Max Planck Institute for Biogeochemistry, Hans-Knöll-Str., 10 D-07745 Jena, Germany
[i] Department of Environmental Science and Policy – ESP, Università degli Studi di Milano Via Celoria Milan, Italy
[j] School of Natural Resources, University of Nebraska-Lincoln, Lincoln, NE 68583-0961, USA
[k] Department of Earth and Atmospheric Sciences, University of Alberta, Edmonton, AB T6G 2E3, Canada
[l] European Commission, Joint Research Centre, Ispra, VA, Italy
[m] Swiss Federal Institute for Forest, Snow and Landscape Research (WSL), Forest Dynamics, Birmensdorf, Switzerland
[n] Forschungszentrum Jülich GmbH (FZJ) – Juelich Research Center, Jülich, Wilhelm-Johnen-Straße 1, 52428, Germany
[o] European Space Agency, ESTEC, Noordwijk, Netherlands
[p] International Institute for Earth System Sciences, Jiangsu Center for Collaborative Innovation in Geographical Information Resource Development and Application, Nanjing University, Nanjing 210023, China

ARTICLE INFO

Keywords:
Field spectrometer
Sentinel-2
Time series
Cloud filtering
Data fusion
FloX
RoX

ABSTRACT

Sentinel-2 satellite data enables multispectral monitoring of the earth at a high temporal revisit rate. Combining this information with a network of optical ground measurements enables a more detailed and a more complete understanding of terrestrial ecosystems. However, independent optical ground measurements often lack consistency, especially when comparing different sites in geographically remote locations. Using the very high temporal and spectral resolution offered by the automated field spectrometer systems FloX and RoX (Fluorescence Box and Reflectance Box, respectively, JB-Hyperspectral Devices GmbH, Duesseldorf, Germany), we investigated continuous time series ranging over three years and in ten different locations across Europe, Africa, America and Asia. The continuous records of ground-measured reflectance were first validated against Sentinel-2 top of canopy (TOC) reflectance to evaluate the consistency of the in-situ network. Our results suggest a good agreement of ground-measured reflectance with Sentinel-2 TOC reflectance in vegetation and snow with R^2 around 0.79 in the 833 nm band and R^2 up to 0.94 in the bands around 559 nm and 492 nm, demonstrating good consistency across the network. Spatial misalignment of Sentinel-2 pixel-sizes with respect to the different footprint sizes of the ten automated spectrometers on the ground, atmospheric uncertainties, sub-optimal instrument setup and spatial-temporal variable landscape heterogeneity were identified as the most relevant sources of uncertainties in the network. Comparing the Normalized Difference Vegetation Index (NDVI), Transformed Chlorophyll Absorption in Reflectance Index (TCARI) and Enhanced Vegetation Index (EVI) between ground and satellite revealed a decreasing agreement with increasing complexity of index formulation.

* Corresponding author.
E-mail address: paul@jb-hyperspectral.com (P. Naethe).

https://doi.org/10.1016/j.rse.2024.114013
Received 13 January 2023; Received in revised form 4 January 2024; Accepted 17 January 2024
Available online 25 January 2024

The best agreement between satellite and ground was exhibited by NDVI with R^2 around 0.96 and relative error of 4.3% investigating vegetation and snow across all ten sites. Furthermore, we identified a seasonal pattern in residuals of NDVI between ground and satellite in an alpine ecosystem in northern Italy, which was associated with increased spatial heterogeneity due to the effects of diverse vegetation phenology and snowfall. In contrast, a random distribution of residuals was recognized in a rather uniform oak forest canopy in southern France. Clustering Sentinel-2 pixels with respect to their temporal patterns in NDVI identified similar areas seen as homogenous in the canopy of Torgnon, Italy, and Observatoire de Haute-Provence (OHP), France, each. The very high temporal resolution of NDVI measured on the ground confirmed overlap with matched homogenous areas, but must consider seasonal landscape heterogeneity. Using well-standardized and globally homogenous Sentinel-2 TOC reflectance enabled the assessment of uncertainties in ten field spectrometer sites around the world. The standardization of the automated field spectrometers, their data products and data annotation were essential prerequisites that enabled joint validation against Sentinel-2. Harmonizing optical ground measurements with respect to a satellite is promising for future research to ensure the valid intercomparison and transfer of data products across different sites in a network worldwide.

1. Introduction

Remote sensing of the earth's terrestrial surface from satellites provides a valuable source of information, often combined with insight from ground-based sensors across scales and domains (Bioucas-Dias et al., 2013). With the Copernicus program, the European Space Agency (ESA) has launched seven Sentinel satellite missions up to now. ESA's Sentinel-2 (S-2) program has two satellites in operation with the primary objective to retrieve high-resolution, multispectral images with a high temporal revisit rate (Drusch et al., 2012). The multispectral configuration is suitable to examine land surface properties, especially for the investigation of coastal waters, land-cover and vegetation (Ariza et al., 2018; Caballero et al., 2020; Hank et al., 2018; Ma et al., 2019; Oxoli et al., 2020; Vincini et al., 2016). Surface reflectance is provided at the bottom of the atmosphere using an atmospheric correction and automated data processing, which is further supported through cloud masks and cloud shadow masks (Baetens et al., 2019). Due to the high temporal resolution and good spectral coverage of the S-2 visible to near- infrared (VIS-NIR) spectral range, this satellite mission is especially suitable to compare with a network of identically specified, automated spectrometer systems, installed in various locations for long periods of time (Wang et al., 2018). Extended time series not only reveal specific spectral signals from different types of land cover, but also provide unique temporal signatures, suitable for change detection of land use classes and inferring plant functional traits (Debella-Gilo and Gjertsen, 2021; Ma et al., 2019). Both, advanced experimental and modelling analyses are of high value for predicting environmental phenomena, for example in estimating burned areas or eroded soil (Lense et al., 2023; Mohammad et al., 2023). Extended time series are particularly useful when temporal and spectral signatures are compared between ground and satellite (Nagai et al., 2020; Sefrin et al., 2021). Especially interesting for the purpose of this study is the unprecedented investigation of the highly consolidated S-2 data for validating and harmonizing a worldwide network of standardized, automated field spectrometers.

Autonomous field spectrometer systems have been increasingly used for the continuous long-term monitoring of vegetation, water, atmosphere and snow (Campbell et al., 2019; Cogliati et al., 2015; Kokhanovsky et al., 2021; Meroni et al., 2011; Naethe et al., 2020; Wagner et al., 2018). While the field spectrometer system FloX (Fluorescence Box) by JB Hyperspectral Devices, Düsseldorf, Germany, was designed primarily for the retrieval of sun-induced chlorophyll fluorescence, both, FloX and RoX (Reflectance Box) share the identical optical configuration in VIS-NIR and are suitable for the retrieval of hyperspectral reflectance and vegetation indices (VI) (Acebron et al., 2021; Burkart et al., 2015b; Dechant et al., 2022; Julitta et al., 2016; Krämer et al., 2021; Mohammed et al., 2019; Siegmann et al., 2021; Vargas et al., 2020). High temporal resolution in combination with the high hyperspectral resolution enable investigation of detailed temporal patterns, both, in VI and reflectance with regards to a very defined field of view (FOV) in one location (Martini et al., 2022). Standardization of spectral ground measurements using automated point-spectrometers has been a longstanding challenge in the field of remote sensing (Cavender-Bares et al., 2020; Gamon, 2015; Milton et al., 2007). Standardized hardware as well as standardized calibration, data processing, data annotation and traceability including uncertainty budgets are necessary to transfer calibrated data in absolute physical unit across a network of instruments (Buman et al., 2022; Hueni et al., 2017; Porcar-Castell et al., 2015). The automated spectrometers investigated in this study fulfilled those requirements and, therefore, could be considered a network. On the one hand, such a network allows to investigate spatial-temporal dynamics at a larger scale worldwide. However, verification of those ground measurements with respect to a globally aligned reference is indispensable for combining insights of great temporal and spectral details across the network and harmonizing data products on the other hand.

Numerous networks and communities were established in the past with the aim to provide a standardized approach to spectral ground measurements, for the purpose of calibration and validation of satellite data, e.g. Aerosol Robotic Network - AERONET (Li et al., 2018) and Spectral Network - SpecNet (Gamon, 2015; Gamon et al., 2006), and to facilitate these optical measurements in the context of a network of carbon flux sites (FLUXNET)(Gamon et al., 2010) such as the Integrated Carbon Observation System (ICOS) (Etzold et al., 2022; Gielen et al., 2017) and the National Science Foundation's National Ecological Observatory Network (NEON) (Ma et al., 2022; Metzger et al., 2019). Ground measurements of ecosystem parameters are important for the understanding, modelling and forecasting of natural phenomena broadly speaking, which globally interlink vegetation dynamics and primary production with the water cycle, carbon cycle and local micrometeorology (Lama et al., 2021a, 2021b; Migliavacca et al., 2017; Norton et al., 2019; Pirone et al., 2023; Rossini et al., 2010). In the context of those existing networks are automated, temporally dense, hyperspectral ground measurements of down-welling and up-welling light interesting, because optical in-situ measurements oftentimes serve as proxies for local ecosystem status parameters and enable the fusion of multiple optical sensors across scales (Naethe et al., 2023; Pérez-Harguindeguy et al., 2013).

Due to rapid changes in the atmosphere and low light conditions, ground-based spectroscopy measurements under cloudy conditions are challenging but valuable for enabling specific insights at the same time (Buman et al., 2022; Kanniah et al., 2012; Kaskaoutis et al., 2008). Optical satellite images are adversely affected by clouds so that cloud-covered areas are unusable and typically masked out, making impossible to observe vegetation canopies under cloudy conditions with optical satellites (Baetens et al., 2019; Petitjean and Weber, 2014). Shadows of clouds and large structures are an increasing issue with increasing spatial resolution of remote sensing images (Liu et al., 2017; Shahtahmassebi et al., 2013). While being especially challenging at lower levels, e.g. on drones and on the ground, effective shadow detection methods are essential for robust data filtering, as remote

sensing products such as reflectance or VI are substantially biased under shadows (Adler-Golden et al., 2002; Damm et al., 2015; Liu et al., 2017; Wemett et al., 2009). However, often studies investigate a limited area only where local cloud-shadow detection on the ground would be sufficient. However, robust cloud detection and filtering are mandatory prerequisites for validating and harmonizing information of multiple optical sensors across scales and domains.

This study used data from S-2 as a reference for validating a worldwide network of standardized field spectrometers and for harmonizing their data products. For the first time, satellite TOC data was used to validate continuous time series of reflectance measured from automated field spectrometers at very high temporal resolution in 10 different locations around the world. We use the very high temporal resolution of ground-measured down-welling radiance to investigate suitable cloud-shadow detection. Reversing the common practice of cross-validating in-situ point-spectroscopy and airborne imaging spectroscopy, as presented in Hueni et al. (2017), 10 identically equipped field spectrometer sites were harmonized and challenges of temporal variability in spatial heterogeneity were unveiled. Considering that S-2 offers global coverage of highly standardized data products, this satellite data served as a stable reference for the independent validation of each site and investigation of site-specific uncertainties in continuous time series recorded by standardized field spectrometer systems over several years on the ground.

2. Materials and methods

We compared dense, hyperspectral time series recorded with FloX and RoX spectrometers in ten different locations in Africa, America, Asia and Europe with time series extracted from simultaneous S-2 overpasses. Combining ground measured and satellite measured data is challenging due to rapid changes in the atmosphere. Therefore, we applied cloud filtering based on both, S-2 cloud masks and on a novel approach using ground-based measurements of incoming light. Top of Canopy (TOC) Reflectance, Normalized Difference Vegetation Index (NDVI) (Tucker, 1979), Enhanced Vegetation Index (EVI) (Liu and Huete, 1995) and the Transformed Chlorophyll Absorption in Reflectance Index (TCARI) (Haboudane et al., 2002) were compared under cloud-free conditions. TOC reflectance was used for absolute and quantitative comparison per spectral band, extracted from satellite and convolved from hyperspectral ground measurements. NDVI is very robust against diurnally variable amounts of solar radiation on the ground and is not sensitive for short-term variations in plant's physiological adaptation processes due to its band selection and formulation (Gamon et al., 1992, 2015), and was therefore considered ideal to compare ground and satellite data. EVI is a more complex modification of NDVI that minimizes effects of soil and atmosphere, which is still mostly stable throughout the diurnal cycle and was considered for that reason. TCARI was used as a more modern, very complex soil-adjusted chlorophyll index, which predicts canopy chlorophyll content regardless of the background of changing land cover (Herrmann et al., 2010; Main et al., 2011). NDVI, EVI and TCARI were feasible to compute from the available S-2 bands in this study and were used to examine the effects of increasing complexity of VI affecting the agreement between ground and satellite data. Finally, the robust NDVI was used to investigate further temporal and spatial aspects affecting the direct validation of ground and satellite data.

2.1. Instruments and sites

A variety of different agricultural and natural vegetation canopies as well as snow were monitored with FloX and RoX field spectrometers in ten different sites across Europe, America, Asia and Africa (see Fig. 1). FloX and RoX share in common identical VIS-NIR spectrometers featuring 450 nm – 900 nm spectral range, 1.5 nm full width at half maximum (FWHM) spectral resolution and a hemiconical optical configuration with up-welling light recorded through bare fiber optics with 25° opening angle and down-welling light recorded through a cosine diffusor with a theoretical 180° opening angle (Chang et al., 2021). Time series were recorded completely unattended with a very high temporal resolution up to one measurement per minute, depending on light conditions in the field (Cogliati et al., 2015). Further processing of the data enabled filtering based on standardized, system-internal

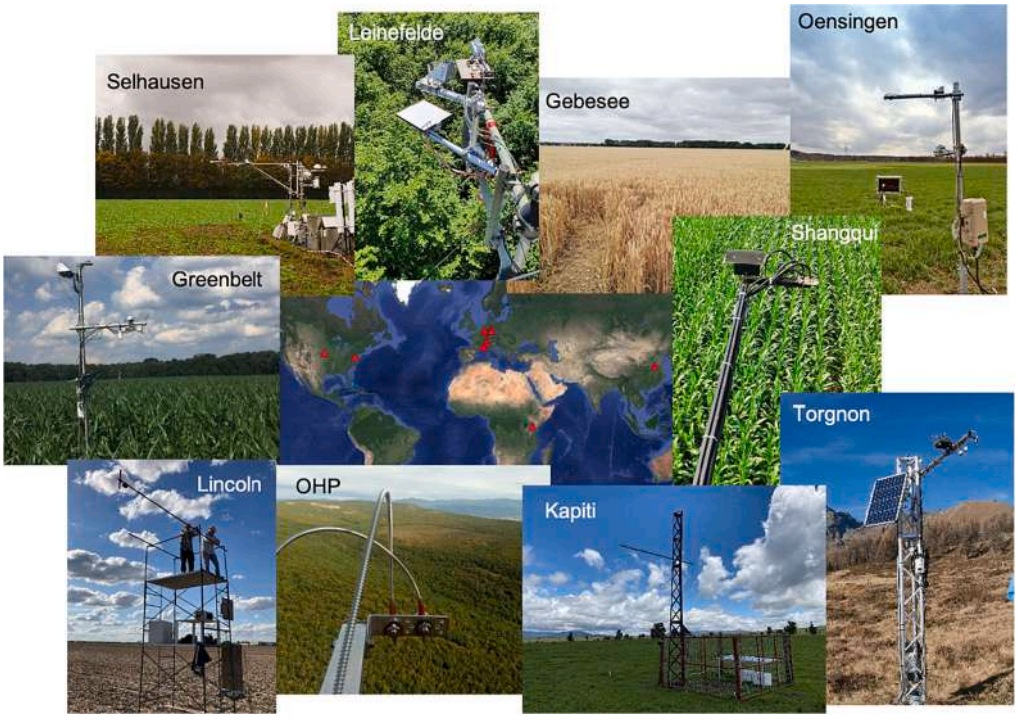

Fig. 1. Selected field sites, equipped with FloX or RoX. Spread over Europe, America, Asia and Africa, covering different vegetation and non-vegetation targets. World Imagery (ESRI, 2021).

quality flags and quantitative parameters indicating goodness of each measurement, accounting for saturation, unstable measurements, automatic optimization and low solar angles.

The ten field sites were set up similarly for the investigation of extended, temporally dense time series of TOC reflectance and VI. For this purpose, all spectrometers were set up on towers in such a way that down-welling light was monitored though the up-facing cosine optics without obstruction from nearby structures. The down-facing bare optics were mounted in a southerly direction (in the southern hemisphere in a northerly direction) on an extended arm to minimize self-shading and ensure unobstructed nadir view onto the desired footprint. Details to the sites, spectrometers and installations are provided in Table 1. The shortest time series covers 6 months and the longest over 3 years of continuous data recording, for which representative parts were selected. An important criterion for the selection of data was the temporal agreement with available S-2 overpasses. Furthermore, ambient light conditions and instrumental quality criteria, as described in the following section were considered for the selection of ground measured data.

2.2. Data processing, cloud detection and statistical analyses

The data from S-2 and from the automated spectrometer network were pre-processed to enable their joint use for cloud detection and filtering (Fig. 2). Finally, only data pairs from ground and satellite filtered and validated as cloud-free using down-welling radiance fitting from the ground were used for further analyses. Each of the steps are described in detail below.

2.2.1. Sentinel-2 preprocessing

Satellite data were selected to match the exact position of the footprint recorded by the automated spectrometers based on the natively annotated GPS-coordinates. The level 2-A products from the Copernicus hub were downloaded and time series extracted for the single pixel at the positions of the spectrometer footprint, a 3 × 3 pixel matrix and a subset of ca. 200 pixels for each site around the instrument using Google Earth Engine (Gorelick et al., 2017). Atmospherically corrected TOC reflectance using the Sen2Cor algorithm included cubic spline resampling (Li et al., 2018) was extracted at 10 m spatial resolution for those S-2 bands overlapping with the spectral range of the field spectrometers between 450 nm and 900 nm shown in Table 2. VIs were computed directly from the S-2 reflectance bands at 10 m spatial resolution in the same way as for ground measurements according to Table 3.

2.2.2. FloX and RoX preprocessing

Raw data from the field spectrometer systems were processed to retrieve calibrated radiance and surface reflectance using the packages FieldSpectroscopyCC (https://github.com/tommasojulitta/FieldSpectroscopyCC) and FieldSpectroscopyDP (https://github.com/tommasojulitta/FieldSpectroscopyDP) with the statistical computing software R (R Core Team, 2017). The hyperspectral reflectance was then convolved to match the multispectral characteristics of S-2 (Table 2) within the VIS-NIR spectral range of FloX and RoX, using Gaussian convolution. Only band 2 to band 8 of the total 13 multispectral bands from S-2 were covered in the convolution, considering the central wavelength and full width at half maximum (FWHM) in each band, which were respectively overlapping with the usable spectral range between 450 nm and 900 nm of the automated field spectrometers. NDVI, EVI and TCARI were calculated for FloX and RoX from the convoluted spectral bands according to Table 3 in order to properly match with the S-2-based products.

The spectrometer data were filtered according to Cogliati et al. (2015) to eliminate unstable, saturated spectra and measurements at

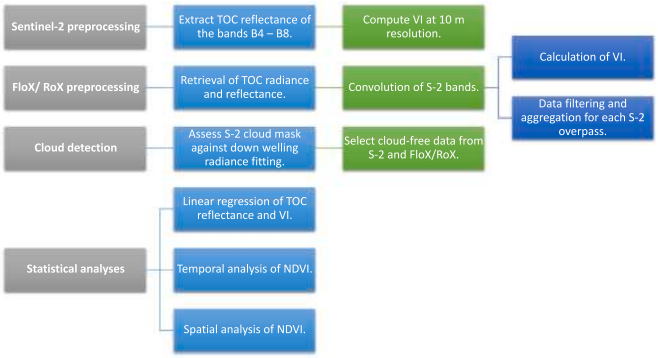

Fig. 2. Schematic of data processing and analyses conducted during this study.

Table 2
Sentinel-2 B bands used for TOC reflectance extraction overlapping with the spectral range of the ground instruments.

Sentinel-2 band name	B2	B3	B4	B5	B6	B7	B8
Central wavelength	492 nm	559 nm	665 nm	704 m	740 nm	780 nm	833 nm
Band width	65 nm	35 nm	31 nm	15 nm	13 nm	19 nm	104 nm
Pixel size on ground	10 m	10 m	10 m	20 m	20 m	20 m	10 m

Table 3
Index formulations used for the calculation from Sentinel-2 multispectral bands and convoluted bands from field spectrometers identified by their central wavelength.

Index name	Formula
NDVI	$\frac{(R_{833} - R_{665})}{(R_{833} + R_{665})}$
EVI	$2.5 \times \frac{(R_{833} - R_{670})}{(R_{833} + 6 \times R_{665} - 7.5 \times R_{492} + 1)}$
TCARI	$\frac{3 \times (R_{704} - R_{665}) - 0.2 \times (R_{704} - R_{559}) \times R_{704}/R_{665}}{1.16 \times (R_{833} - R_{665})/(R_{833} + R_{665} + 0.16)}$

Table 1
Experimental setup giving site name, country, coordinates, spectrometer incl. serial number, site and installation description, target, period investigated.

Site name	Country	Lat	Lon	Target	Dist. from TOC	Footprint radius	Period investigated
Torgnon	Italy	45.844	7.578	Alpine pasture	2 m	0.4 m	06 Dec 2017–05 Mar 2021
OHP	France	43.934	5.711	Oak forest	90 m	20.0 m	06 Dec 2017–16 Sep 2020
Leinefelde	Germany	51.327	10.367	Mixed broadleaf forest	8 m	1.8 m	12 May 2019–03 Oct 2020
Gebesee	Germany	51.100	10.914	Wheat field	2 m	0.4 m	15 Apr 2019–07 Jul 2019
Kapiti	Kenya	−16.144	37.133	Savannah	4.5 m	1.0 m	01 Oct 2019–12 Jul 2020
Lincoln	USA	41.179	−96.441	Corn field	2 m	0.4 m	02 Sep 2019–17 Oct 2019
Greenbelt	USA	39.029	−76.843	Corn field	2 m	0.4 m	25 Jul 2020–24 Aug 2020
Shangqui	China	34.515	115.59	Corn field	4 m	0.9 m	08 Jul 2020–16 Nov 2020
Oensingen	Switzerland	47.286	7.733	Corn field	2 m	0.4 m	25 Jul 2020–24 Aug 2020
Selhausen	Germany	50.865	6.447	Grassland	2 m	0.4 m	18 Nov 2020–27 Apr 2021

low solar zenith angles. In addition, outliers of negative NDVI were identified as measurements of snow and verified as such by time and place of recording. Data were extracted from the continuous time series at a temporal resolution per ca. 1 min using a 20-min time-window around each Sentinel-2 (S-2) overpass and aggregating by the mean of the reflectance and VI values within each time-window.

2.2.3. Cloud detection

Two independent routines were used for cloud detection eliminating cloud-shaded data.

The first filtering routine was based on the S-2-inherent cloud masks (Baetens et al., 2019). Data above 0% cloud coverage were excluded, as fractional cloud cover could not be consistently checked otherwise.

A second filtering routine was applied using dense temporal information of down-welling radiance from ground measurements. The method was based on the assumption that incoming light can be considered stable enough to be expressed by a linear model for a short time period. Thus, a time window of 20 min was selected around the time of the S-2 overpass. A linear model was fitted to the down-welling radiance at 750 nm within this time window. The down-welling radiance within this time-window varied a lot during cloudy conditions, resulting in a poor fit of the linear model with the down-welling radiance and a low correlation coefficient R^2 (see Fig. 3a). Conversely, under clear sky conditions the linear fit resulted in a high correlation with the measured down-welling radiance (see Fig. 3b). Applying ground-based cloud detection, we investigated pairs of S-2 and ground data under clear-sky conditions only.

2.2.4. Statistical analyses

TOC reflectance and VI from S-2 were compared with ground measurements by using linear regression of a 3 × 3 pixel matrix around the position of ground measurements to ensure fully covering the spectrometer footprint. The S-2 pixels were summarized by their mean value around the position of the field spectrometer. The coefficient of determination (R^2), the confidence of significance (p-value) and slope were computed for each linear regression of reflectance bands and VI, respectively. In addition, the root mean square error (RMSE, eq. 1) and relative RMSE (RRMSE, eq. 2) in percent were calculated, using $\hat{x}$ as the measured reflectance or VI from S-2 and x as the measured reflectance or VI from FloX/ RoX with respect to the total number of n measurements.

$$RMSE = \sqrt{\frac{\sum_{i=1}^{n}(\hat{x}_i - x_i)^2}{n}} \quad (1)$$

$$RRMSE = \frac{\sqrt{\sum_{i=1}^{n}(\hat{x}_i - x_i)^2}}{\sum_{i=1}^{n}\hat{x}_i} \cdot 100\% \quad (2)$$

Also, the temporal residuals in NDVI were calculated as the difference between satellite and ground measurements for each data pair in the entire time series. A histogram of the residuals was created to investigate their distributions. Furtermore, median and standard deviation (sd) were calculated.

Finally, spatial clustering using the "tsclust" algorithm from the "dtwclust" R-package (https://github.com/asardaes/dtwclust) was conducted on each pixel of the subset (ca. 200 pixels) around the automated field spectrometers. Hierarchical clustering of NDVI time series per pixel was performed in the two three-years-long datasets. The time series of NDVI pixels were grouped into three clusters based on normalized dynamic time warping distances (Aghabozorgi et al., 2015; Wallace and Dale, 2005).

Pixels of similar temporal patterns in NDVI around the location of ground measurements were identified and allocated in 3 groups by the algorithm (Fig. 4). The depth of differentiation of the clusters was indicated by the relative distance of the top node of each cluster. Note that the NDVI pixels from the canopy in Torgnon were identified more

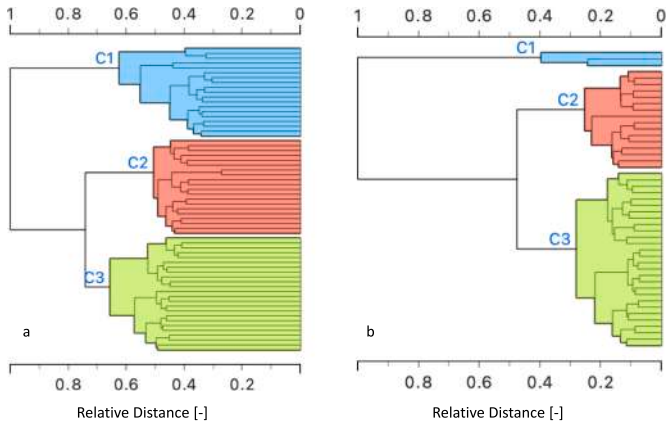

Fig. 4. Cluster dendrogram from the hierarchical clustering of NDVI time series associated with a pixel of the subset each in Torgnon (a) and OHP (b). Clusters C1, C2 and C3 are marked each in a different colour. The tree depth is given in relative Euclidian distance between 0 and 1. The leaves correspond to pixel IDs in the mosaics. Note that the level of displaying was pruned and not all pixels are listed for improved readability, pruning to a maximum depth of 7.

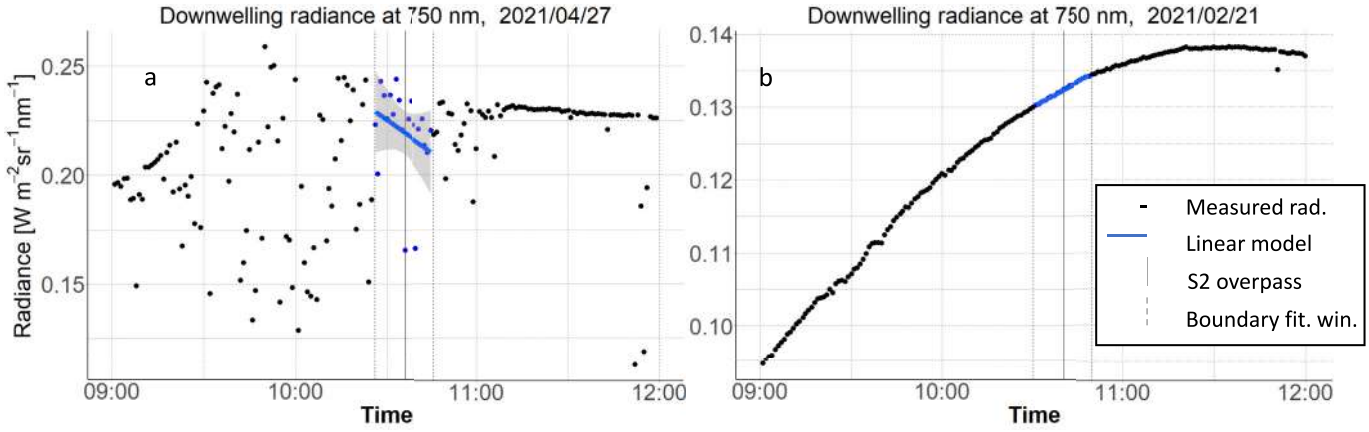

Fig. 3. Principle of data filtering approach based on downwelling radiance. Diurnal course of cloudy incident radiance (a) compared to clear incident radiance (b). Measurements are printed in black while the linear fit is printed in blue, dashed grey vertical lines indicate the 20 min. Time-window around the S-2 overpass, which is marked by a solid grey line. (For interpretation of the references to colour in this figure legend, the reader is referred to the web version of this article.)

diverse than those from OHP, accordingly. Finally, the temporal patterns in each cluster were compared with the ground measured temporal patterns. A visual inspection was conducted comparing the location of pixels associated to each cluster with respect to the location of ground measurements for both sites. Agreement of the clusters of NDVI pixels with respect to the spectrometer footprint verified temporal and spatial representativeness of the ground measurements for the area covered by clustered pixels.

3. Results

3.1. Cloud filtering

Filtering by ground-measured down-welling radiance fitting was applied to deselect clouded satellite data of overpasses during which the linear fit yielded an R^2 value below 0.7. This resulted in an overall acceptance rate of 49% of the available data pairs from ground and satellite (Fig. 5), compared with an average acceptance rate of 86% using conventional cloud masks. A detailed comparison of retained data using filtering by cloud masks and ground-measured down-welling radiance fitting are provided in Table 4. A significantly larger number of S-2 overpasses was identified cloud-free using cloud masks, but still showed in parts effects of clouds in the ground-measured data within the region of interest (ROI).

Therefore, cloud filtering based on down-welling radiance measurements was considered more conservative and suitable for the further analyses compared to S-2 cloud masks. Since the S-2 cloud-mask included also data pairs which were evidently affected by clouds, the ground-based filtering was used for all further investigation.

3.2. Spectral reflectance and VI

Ground measured and satellite measured reflectance were compared for all eight multispectral bands, which fell within the spectral range of FloX and RoX. To visually compare measurements across all sites, band 5 around 704 nm, band 6 around 740 nm and band 7 around 780 nm were selected from the central region of the FloX's/RoX's detector (Fig. 6).

A noticeable deviation from a slope of one was exhibited in all panels of Fig. 6. Overall, lower R^2 and larger deviation from a slope around one was recognized in the reflectance bands when excluding measurements

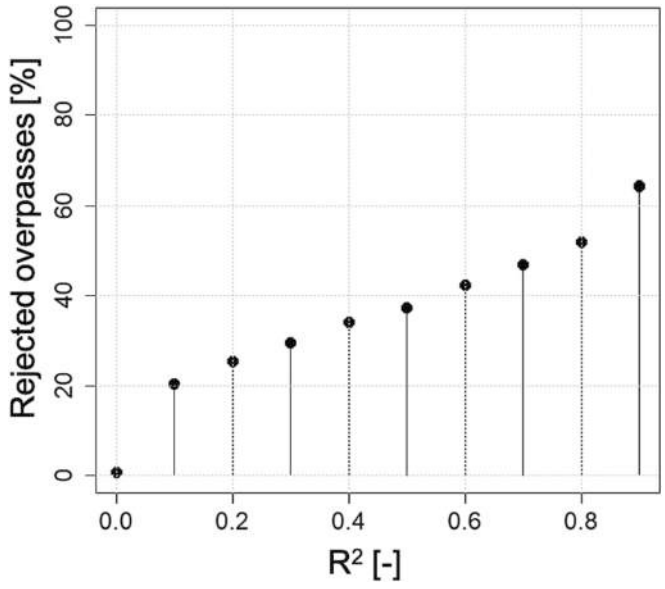

Fig. 5. Rejection rate of all data given in % with respect to changing R^2 of the linear fit for ground measurements around the S-2 overpass set as threshold for filtering cloudy conditions.

Table 4
Number of Sentinel-2 overpasses paired with ground measurements available for each site in total and after the filtering using Sentine-2 cloud mask or ground measured incoming radiance, respectively.

Sites	All Sentinel-2 overpasses paired with ground measurements	Remaining instances filtered by Sentinel-2 cloud mask	Remaining instances filtered by down-welling radiance
Gebese	15	14	7
Kapiti	14	11	3
Leinefelde	44	36	14
Greenbelt	8	8	6
Lincoln	23	22	7
Shangqui	7	7	3
OHP	105	100	67
Selhausen	7	6	3
Oensingen	14	12	5
Torgnon	169	133	94

of snow. Likewise, a smaller dynamic range of reflectance was recognized for pure vegetation samples only. Noticeable outliers with respect to the regression's trendline were noticed for the field sites in Linefelde, affected by the off-nadir tilted up-welling optics and for some recordings of snow in Torgnon, both of which were affected by reflection hotspots in the target. Reflection hotspots in the snow caused reflecting direct sunlight, which entered the downwards facing optics of the instrument. This is a known issue of snow, caused by a series of variables related to acquisition, illumination geometry, and surface topography. Taking a purely diffuse reference for the down-welling light using cosine diffusors in combination with direct sunlight in the up-welling resulted in a calculated reflectance greater 1, which must be understood as an artifact.

A detailed assessment of each band is reported in Table 5. The coefficient of determination between satellite-measured and ground-measured reflectance varied a lot between the different multispectral bands across all sites. The lowest coefficient of determination was recognized in band 6 around 740 nm with R^2 of 0.45, a slope of 0.67 and RRMSE around 4.8%, as well as in band 8 around 833 nm with R^2 of 0.45, a slope of 0.71 and relative RMSE around 5.5% in the subset of vegetation only. Taking also reflectance of snow into account, all R^2 values increased significantly. Due to a higher variance and covariance in the data also the absolute and relative error increased (Fig. 6). The RMSE increased almost consistently with increasing wavelength of the multispectral bands. The RRMSE was affected by the typical reflectance shape of pure vegetation targets, resulting in higher relative values for visible wavelength at lower intensities and in lower relative error of near-infrared wavelength of higher intensities (compare Fig. 7 and Table 5). The RRMSE values were more similar across all spectral bands when including snow, since a larger diversity of non-vegetative spectral reflectance shapes was introduced in addition to a larger variance of reflectance. Lowest coefficient of determination was recognized in band 8 around 833 nm in the dataset including snow with R^2 of 0.79, slope of 0.66 and a RRMSE of 2.8%. This is half of the RRMSE value compared to data including vegetation only. When including snow, the agreement for the bands up to band 5 were very good with R^2 above 0.9 and RRMSE between 3.1% and 7.5%. All reported results were significant according to a 99.9% confidence interval, applying the *p*-value test.

Good agreement was recognized in the reflectance shape between the two platforms (see Fig. 7). Especially the spectral shape typical for vegetation was well retained in the selected cases. A very clear seasonal pattern in the relative differences between satellite-based reflectance and ground-based reflectance was observed in Fig. 7 especially at OHP. In contrast, the relative discrepancy was more evenly distributed in Torgnon across the temporal domain and exhibited less seasonality due to a lack of usable data pairs during winter. Most stable across the temporal domain was the band around 780 nm for both Torgnon and OHP, yielding the lowest associated relative RMSE in pure vegetation

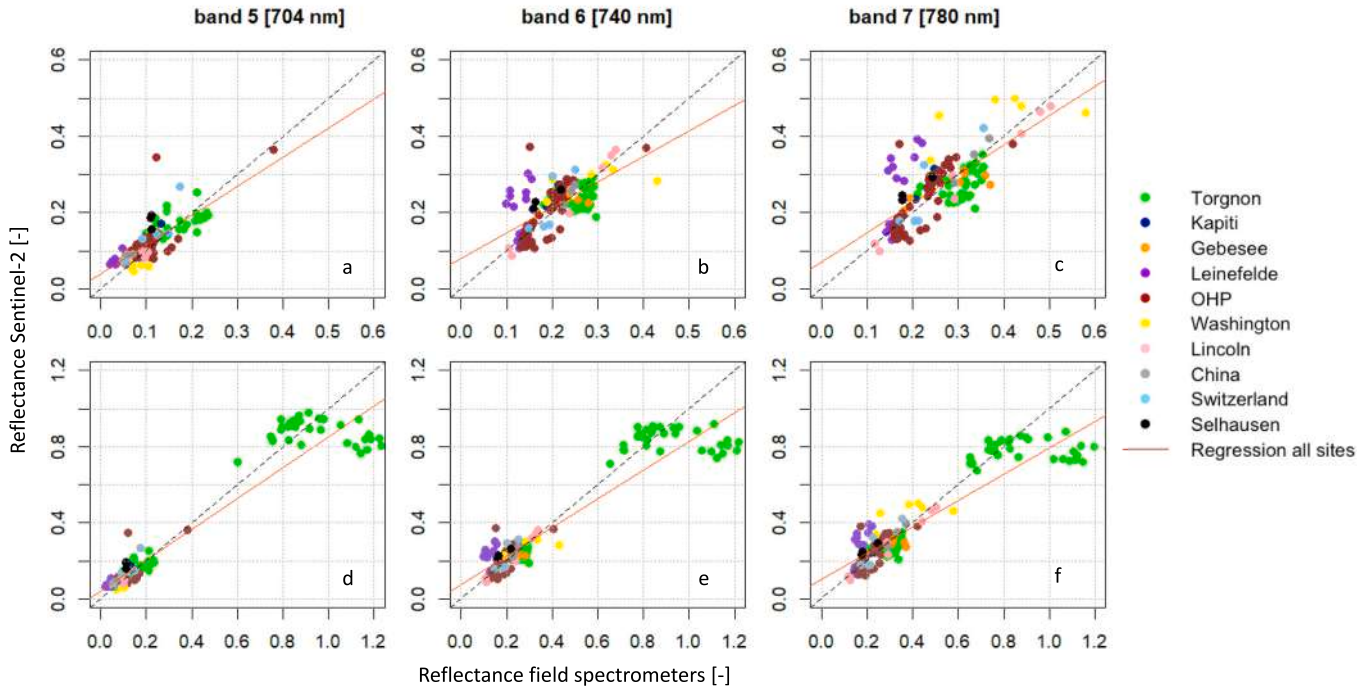

Fig. 6. Scatterplots show reflectance at bands around 704 nm, 740 nm and 780 nm from Rox/FloX vs Sentinel-2 measurements, respectively. Data in panels a, b and c excludes measurements of snow, in panels d, e and f are results for all measurements displayed. Regression line in dashed red indicates deviation from line of identity in dashed black. (For interpretation of the references to colour in this figure legend, the reader is referred to the web version of this article.)

Table 5
Correlation between satellite-measured and ground-measured reflectance. Statistics shown of regression for the different bands (only for rigorous filtering), p-value, RMSE, %-RRMSE, across all sites vegetation only and included snow, respectively.

Bands	R Squared	*P* Value	Slope	rmse	% RRMSE
vegetation only					
492 nm	0.59	<0.01	0.91	0.023	11.82
559 nm	0.58	<0.01	0.84	0.025	10.73
665 nm	0.72	<0.01	0.89	0.029	11.56
704 nm	0.59	<0.01	0.76	0.035	11.65
740 nm	0.45	<0.01	0.67	0.051	4.79
780 nm	0.53	<0.01	0.77	0.061	4.10
833 nm	0.45	<0.01	0.71	0.065	5.48
Including Snow					
492 nm	0.94	<0.01	0.84	0.104	7.47
559 nm	0.94	<0.01	0.83	0.106	6.81
665 nm	0.93	<0.01	0.83	0.105	5.43
704 nm	0.92	<0.01	0.81	0.109	3.06
740 nm	0.88	<0.01	0.75	0.117	4.31
780 nm	0.83	<0.01	0.69	0.127	4.82
833 nm	0.79	<0.01	0.66	0.138	2.79

(compare Fig. 7 and Table 5).

Similar to the investigation of absolute reflectance for individual multispectral bands, VIs were examined for their agreement between ground and satellite measurements. For this purpose, NDVI, EVI and TCARI were computed, both from the convoluted bands of the ground measurements and the multispectral bands of S-2 reflectance, including atmospheric correction. A regression analysis was performed, indicating that NDVI, EVI and TCARI agreed well across both platforms, recognizing a noticeable difference in value range between pure vegetation and measurements including snow, especially in NDVI (Fig. 8). NDVI exhibited a very good coefficient of determination with R^2 around 0.96 (incl. snow) and 0.90 (vegetation only) and a slope close to one (Table 6). The RRMSE was in both cases very similar around 3.8% and 4.3%. Agreement in TCARI values was overall the strongest affected by the snow and performed very differently with R^2 around 0.75 (incl. snow), while the coefficient of determination in pure vegetation targets was reduced to R^2 around 0.55 due to a larger scattering of values. The RRMSE was almost doubled for those measurements which included vegetation only in TCARI, because a larger variance in the data was introduced due to snow (Fig. 8). EVI exhibited a lower coefficient of determination R^2 around 0.88 (incl. snow) between ground and satellite measurements, while the value changed not noticeably to R^2 around 0.86 investigating vegetation targets only. Similar to TCARI, the RRMSE was almost doubled by the exclusion of snow.

Ground measurements and satellite measurements agreed better when examining simple TOC reflectance of the individual bands compared with the more complex EVI and TCARI computed from those bands. The coefficient of determination between ground and satellite measurements decreased with increasing complexity of the index formulation of NDVI, EVI and TCARI, in that order. EVI was by far the most robust index with respect to influences from snow and exhibited the lowest RRMSE, both in pure vegetation and including snow. Due to the highest variance in values with respect to the spread of datapoints around the regression line in Fig. 8, RRMSE of EVI was the lowest. On the contrary, the absolute RMSE was lowest for TCARI in vegetation only and for NDVI including snow.

3.3. *Temporal and spatial patterns*

When investigating the two longest time series (i.e., the time series from OHP and Torgnon), only a fraction of the ground measurements were usable for further analysis. Only S-2 overpasses under cloud-free conditions were used, previously identified by using the down-welling radiance-based filtering. The resulting gaps with respect to the higher temporal resolution of the continuous monitoring using ground measurements were obvious especially in Torgnon in the Alps (Fig. 9). In Torgnon data recorded during winter were filtered out for all three years, due to the exclusion of snow to focus on the analysis of vegetation only. In contrast, a much better coverage of the annual pattern in NDVI was achieved from the ground including all seasons. In OHP in southern

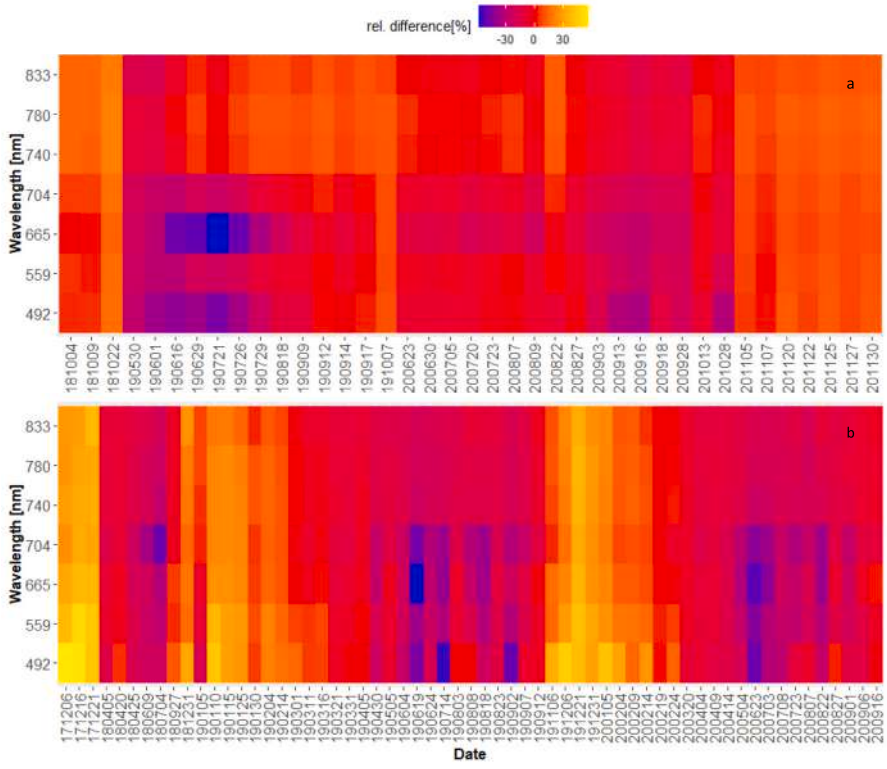

Fig. 7. Heatmap indicating the relative difference percentage (%) of convoluted ground-measured reflectance using autonomous field spectrometers with respect to Sentinel-2 TOC reflectance, covering over three years of investigation in Torgnon (a) and in OHP (b).

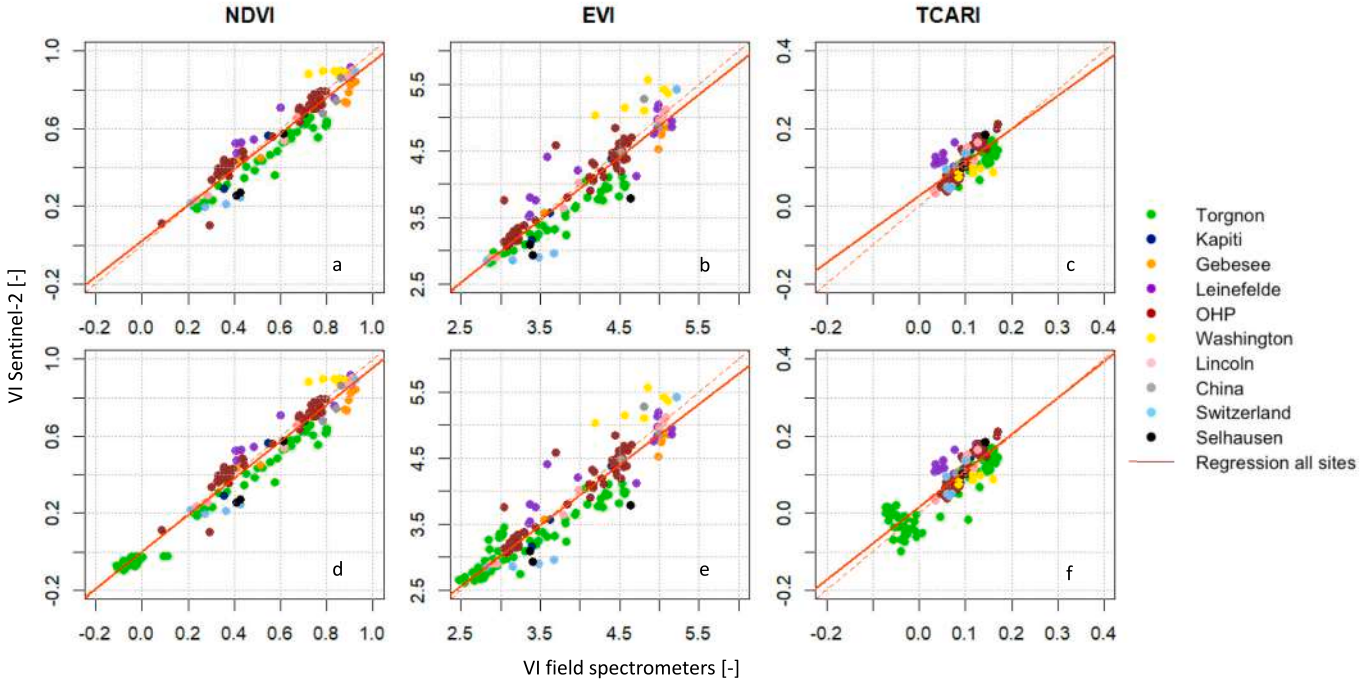

Fig. 8. Comparison of field Rox-Flox and S-2 satellite VIs. Scatterplots show NDVI, EVI and TCARI from Rox/FloX vs Sentinel-2 measurements, respectively. Data in panels a, b and c excludes measurements of snow showing vegetation only. In panels d, e and f are results for all measurements displayed. Regression line in solid red indicates deviation from line of identity in dashed red. (For interpretation of the references to colour in this figure legend, the reader is referred to the web version of this article.)

Table 6
Statistics of regression for the VI (only for radiance-based filtering), *p*-value, RMSE, %-RRMSE, across all sites vegetation only and included snow, respectively.

Indices	R Squared	P Value	Slope	rmse	% RRMSE
VEgetation only					
TCARI	0.55	<0.01	0.88	0.029	11.25
EVI	0.86	<0.01	0.94	0.291	1.41
NDVI	0.90	<0.01	0.93	0.074	3.80
Including Snow					
TCARI	0.75	<0.01	0.83	0.105	5.44
EVI	0.88	<0.01	0.92	0.276	0.76
NDVI	0.96	<0.01	0.96	0.068	4.34

France there were a larger number of S-2 overpasses available throughout the investigated years. However, in both cases the high temporal resolution of the ground measurements depicted annual dynamics to a much better degree compared with satellite measurements. This advantage was especially noticeable during seasons of unstable weather conditions. When stable conditions for reliable measurements were difficult to identity using the S-2 cloud-masks, ground measurement still identified locally usable data.

While the temporal evolution of the discrepancy between ground-measured and satellite-measured NDVI followed a right-skewed, normal distribution centered around zero for all data combined, the residuals were not always normally distributed for individual time series, such as Torgnon (Fig. 10). A median residual NDVI around −0.02 and a standard deviation of 0.09 was recognized across all sites, indicating very low systematic differences between ground and satellite. In particular, median residual NDVI in Torgnon was around −0.06 with a standard deviation around 0.08. In OHP the median discrepancy was below −0.01 with a standard deviation of 0.07. All these values similarly indicated a negligible systematic tendency of underestimating NDVI on the ground, taking S-2 as reference. However, the random uncertainties significantly exceeded those systematic errors. The highest occurring frequency of residual NDVI in ground measurements with respect to the satellite measurements was found by the mode just below zero in all sites (Fig. 10). For the extended two time series the absolute residual NDVI followed the seasonal vegetation cycle in Torgnon, while the residual NDVI in OHP data showed a more random pattern.

Finally, we investigated the pixels in the sub-section around the location of the RoX in Torgnon and the FloX in OHP with respect to spatial similarity of the NDVI. Each pixel exhibited a specific temporal pattern in NDVI and was compared in with all other subset pixels, so that similar temporal patterns would be summarized into a cluster. In Torgnon the clustering algorithm identified three major clusters in the S-2 pixels and associated specific trends in seasonal pattern accordingly (Fig. 11). Those clusters of seasonal patterns were spatially associated with certain spatial features. The seasonal pattern in NDVI recorded by ground measurements in Torgnon was similar to cluster 2 of S-2 based NDVI pixels, at the fringes to cluster 3 during 2018 and 2019 (Fig. 11). Likewise, the position of the RoX was located inside pixels, which were spatially associated to cluster 2 at the border to cluster 3. Similarly, in OHP the algorithm identified three clusters, of which cluster one was the major contributor. The spatial location of the ground measurements at the border between the three clusters resembled the temporal pattern of ground measurements falling into cluster 1 mainly during summer and into cluster 3 mainly during winter. Hence, spatial features were successfully associated with the temporal NDVI patterns from both S-2 and ground measurements.

4. Discussion

4.1. Spectral reflectance and VI

Previous studies have compared reflectance measurements using different spectrometer systems on the ground and also investigated differences in VI across ground and satellite (Castro-Esau et al., 2006; Cheng et al., 2006). Our results suggested a better agreement in absolute values compared with these studies, both in reflectance and in VI comparing FloX/RoX measurements with S-2 TOC products. Thus, TOC reflectance and VI data from the network of 10 FloX and RoX sites were considered very coherent with respect to S-2. Similar to (Cheng et al., 2006), a characteristic seasonal pattern was identified in the relative discrepancy of reflectance bands between ground and satellite in the two longest time series in this study. This seasonal pattern suggested temporal-spatial variabilities of uncertainties with respect to the static and continuous ground measurements, which were investigated more closely in this study using the spatial information available from S-2. Best practice in characterization, traceability and standardization will further enable fusing validated ground data to improve the spectral, temporal and spatial details of future studies. Thus, future efforts would benefit from the accreditation of radiometric calibration routines of FloX and RoX and assure traceability with respect to a fiducial reference

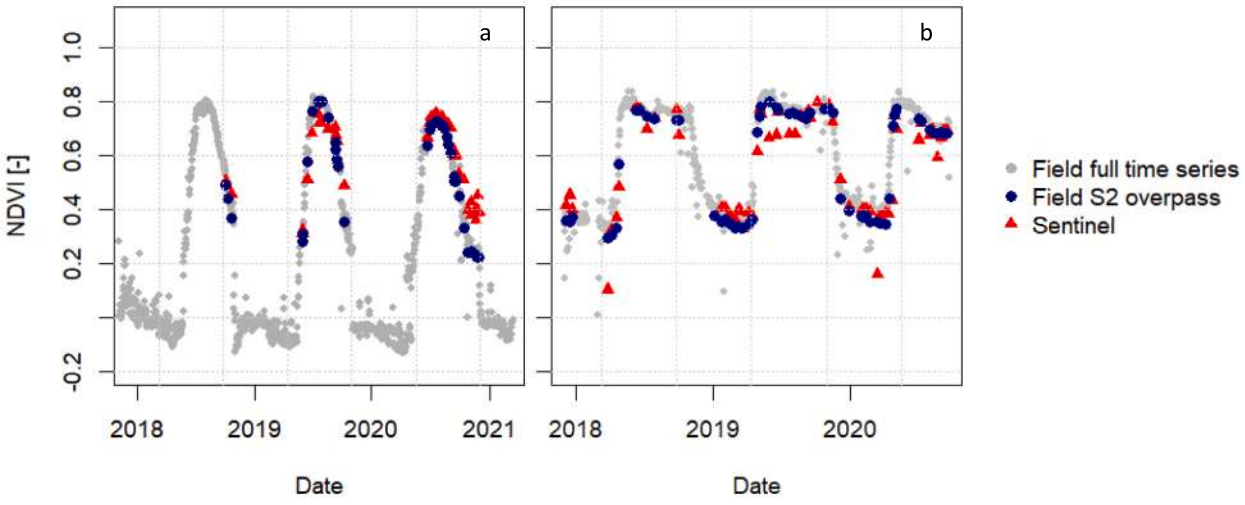

Fig. 9. Time series measured from satellite and on the ground in Torgnon (a) and OHP (b), where data over approximately three years were available. The selected data from a usable satellite overpass (red) is compared with the associated ground measurement (blue). Negative NDVI values were caused by snow. (For interpretation of the references to colour in this figure legend, the reader is referred to the web version of this article.)

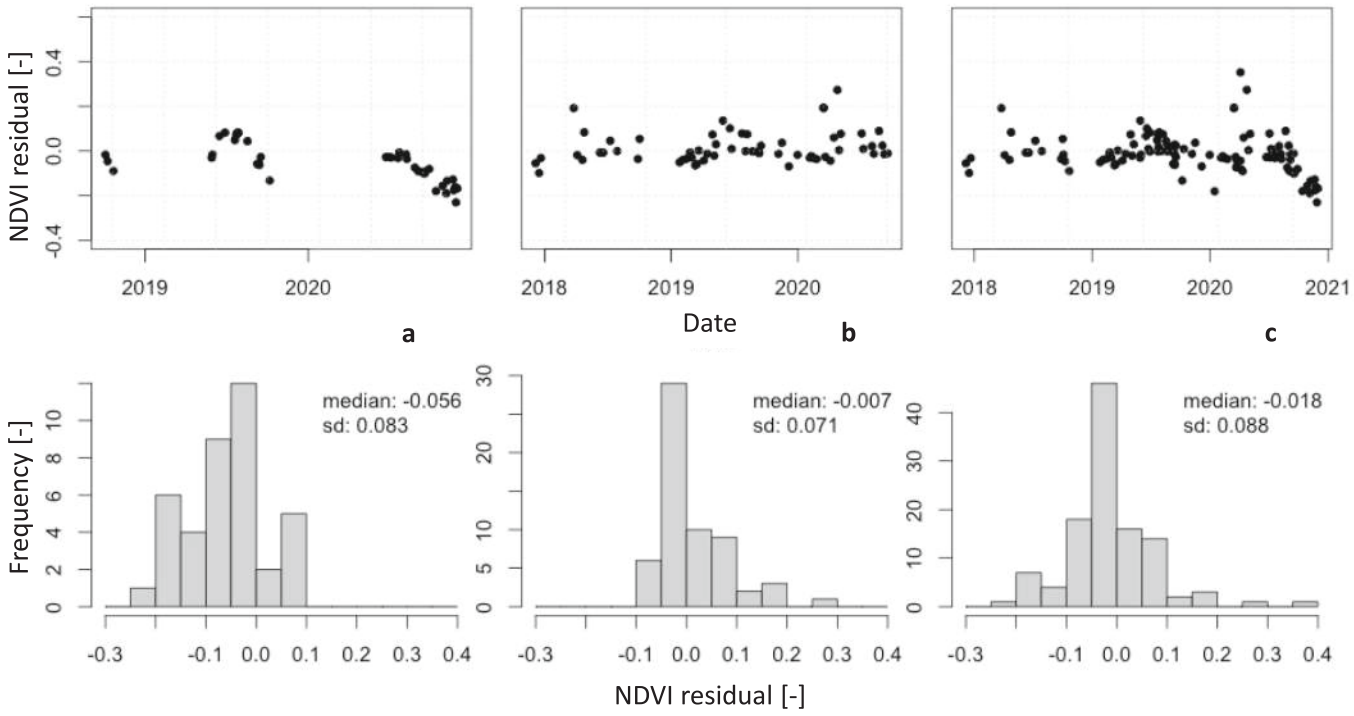

Fig. 10. Residual of NDVI over time (top) and distribution of the residual (bottom) for Torgnon (a), OHP (b), and for all available sites (c).

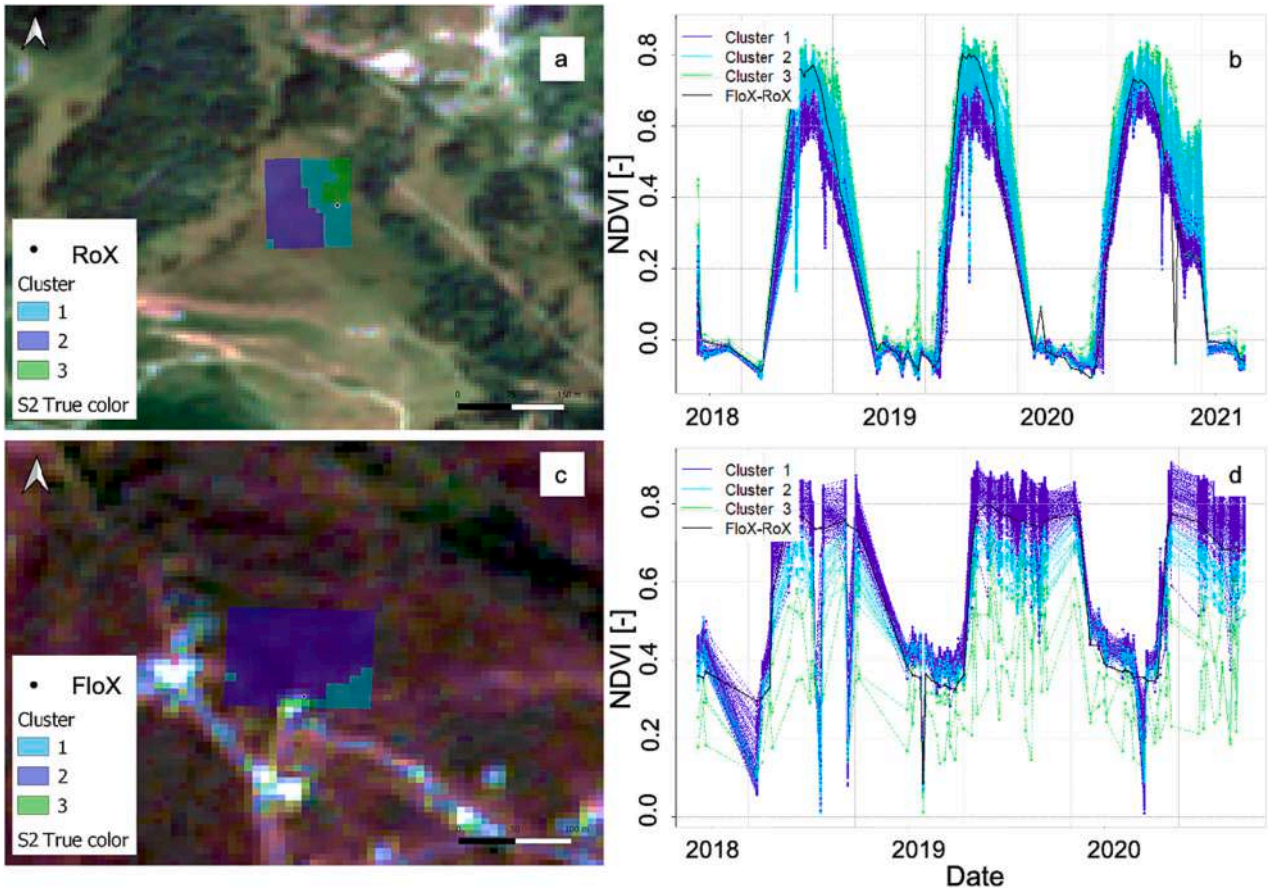

Fig. 11. Time series similarity clustering. Rox/FloX was spatially identified in the associated cluster of similar Sentinel-2 pixels with respect to similar temporal patterns in NDVI. Satellite scene of the ROI in Torgnon, Italy (a) and in OHP, France (c). Clustered time series of NDVI with respect to pixels identified as similar using hierarchical clustering in Torgnon (b) and OHP (d).

(Mihai et al., 2018; Picard et al., 2016; Schaepman and Dangel, 2000). With continuous time series being available from the automated spectrometers, ground-measured data were extracted exactly for the time of the S-2 overpass in order to minimize temporal uncertainties. However, uncertainties around the different spatial resolutions had to be considered, which affected the direct comparison of ground measurements and satellite data (Vogtli et al., 2021; Zagajewski et al., 2017). The varying pixel-sizes of S-2 bands (Drusch et al., 2012) and the varying footprint radius of point spectrometers from 0.5 m to 20 m, depending on the height of installation, limited the best possible agreement between ground and satellite (Milton et al., 2007). In addition, inconsistencies around the setup of the automated field spectrometers yielded another important source for uncertainties. In particular, off-nadir misalignment of the up-welling and down-welling channels of FloX and RoX results in an offset with respect to the satellite TOC reflectance (Drolet et al., 2014; Hueni et al., 2017). Compensation for atmospheric distortion of the light passing from space to the ground is furthermore important for the retrieval of accurate results validated from the satellite (Schläpfer et al., 2020a; Vogtli et al., 2021). While ground measurements by field spectrometers already included the path of light through the atmosphere, S-2 reflectance had to infer these atmospheric influences. We used S-2 TOC reflectance, which was processed using the Sen2Cor algorithm to account for the atmospheric distortion of light (Li et al., 2018). Short-term changes of the atmosphere affect the measurements at the ground level and introduce an additional uncertainty. We tried to address this issue by using a very conservative cloud filtering approach, which aimed to identify those shot-term variations in the atmosphere from the ground. However, some compromises had to be made with respect to retaining a usable amount of data pairs for further analyses. Furthermore, multispectral reflectance was convolved from the hyperspectral ground measurements assuming a Gaussian spectral response of S-2. It has to be noted that this basic assumption is a simplification and the actual spectral response function of S-2 bands is in truth of a more complex shape (Li et al., 2018). Even though the assumption of a Gaussian response did mimic the S-2 multispectral bands closely, it was sufficient for this investigation and introduced only a minor systematic error into the comparison. Combining uncertainties from spatial misalignment, atmospheric correction, radiometric calibration, convolution and setup is essential towards fully characterizing the standardized application of high-resolution hyperspectral ground measurements to be used in fusion with multispectral, imaging satellite sensors (Ariza et al., 2018; Mihai et al., 2018; Schmitt and Zhu, 2016).

The complexity of the VIs affected their behavior in a very distinctive manner in this study. The variance of absolute NDVI values was increased by measurements including snow in contrast to pure vegetation. NDVI is a very widely used VI for the remote sensing of vegetation and is based on the red-edge feature of vegetation (Eitel et al., 2010; Gamon et al., 1995; Yao et al., 2013). Thus, negative NDVI of snow must be considered as an artifact, which affected our presented statistics by increased value range (Wang et al., 2023a). Those artifacts were caused by the specific bi-directional reflectance distribution function of snow due to a series of variables related to acquisition, illumination geometry or surface topography (Painter and Dozier, 2004; Picard et al., 2020). At the same time, the negative NDVI values exhibited by snow were a criterion for filtering only vegetation measurements (Jiang et al., 2006; Wang et al., 2023b). In comparison to the other more complex VIs, NDVI with R^2 exceeding 0.9 and relative error remaining below 5% between satellite and ground measurements suggested a good inter-site transferability on ground and good transferability between ground and satellite. The increased robustness of EVI against influences from soil and atmosphere resulted in less pronounced outliers produced by snow but differentiated more the vegetation between sites (Liu and Huete, 1995). Thus, the absolute error in EVI was the highest of all the three investigated VIs. Also, the formulation of EVI is more complex than NDVI, resulting in singular uncertainties from the individual multispectral bands propagating more strongly (Stow et al., 2019). Considering our results, an adjustment of EVI values would be recommended to harmonize all sites with respect to S-2. Finally, TCARI exhibited lowest coefficient of determination and highest relative error when comparing ground and satellite. Being the most complex of the three investigated VIs, TCARI was designed for canopy chlorophyll prediction and to be robust against impacts from soil (Malenovský et al., 2006). This resulted in TCARI being affected the most by covariances of uncertainties propagated from the spectral reflectance. Future research should investigate appropriate correction approaches especially for TCARI towards improving transfer of information across platforms (Ariza et al., 2018; Olsson et al., 2021), which was beyond the scope of this study. Thus, NDVI was identified as most suitable to further compare temporal and spatial aspects and reduce effects of spectral uncertainties at the same time.

4.2. Temporal and spatial analyses

Temporal patterns in NDVI from ground and satellite were compared for the two longest time series recorded in OHP and Torgnon. Both locations provided data recorded over three years. The absolute difference in NDVI between the platforms over time exhibited a seasonal pattern in Torgnon, which had to be compared to a random pattern in OHP. It is followed that the systematic seasonal discrepancy pattern was caused by snowfall and diverse vegetation phenology in the highly dynamic alpine ecosystem (Alberton et al., 2017; Fu et al., 2014; Peano et al., 2021), leading to an increased fractional heterogeneity of the landscape during fall and spring. Heterogeneity of the canopy also increased during certain growth stages and added further spatial uncertainties (Pieruschka et al., 2014). At the same time, larger solar zenith angles during spring and fall can drive bidirectional reflectance artifacts and introduce uncertainties into reflectance of snow measured from ground (Ball et al., 2015). This is especially obvious for those instances of reflectance >1 measured on the ground, caused by reflected direct sunlight in the up-welling with respect to a totally diffuse down-welling reference. We addressed this issue partially by filtering the ground measurements for solar zenith angle below 75°, but could not rule out bidirectional reflectance artifacts driven by surface anisotropy. Furthermore, additional uncertainties were introduced by the circumstance that satellite measurement varied in viewing angle depending on the position of the ROI in the swath width over both sites, as the bidirectional distribution of reflectance varies significantly in natural canopies (Aasen and Bolten, 2018; Burkart et al., 2015a). This effect is very difficult to assess from the satellite scale and would require a thorough investigation of bidirectional reflectance distribution using goniometers or drones on the ground (Biriukova et al., 2020; Honkavaara and Khoramshahi, 2018; Stow et al., 2019), which was beyond the scope of this study. Investigating spatial uncertainties related to canopy characteristics using spatial clustering is promising (Rejichi and Chaabane, 2015). We investigated spatial homogeneity at satellite level, clustering similar pixels of the subset pixels with respect to their temporal pattern in NDVI. The footprint of the ground measurements in OHP was equal or larger than the S-2 pixel size. This large footprint minimized influences of individual plants and other smaller features. Thus, canopy characteristics were assumed as spatially homogenous for that integrated footprint (Jiang et al., 2006). The same assumption was made for the equally large ground-projection of the S-2-pixel size. In consequence of the rather homogenous canopy in OHP, the algorithm identified the largest number of similar pixels within one cluster but at a shallow depth of differentiation. Thus, it was followed that larger areas could be seen as homogenous and provided little spatial diversity at that scale. This reasoning is supported by the median residual in NDVI between ground and satellite around 0 in OHP. In contrast, the canopy in Torgnon was identified as more diverse, indicated by the 3 larger clusters at greater depth of differentiation. It is noteworthy that the spectrometer footprint on the ground was integrating a smaller area in Torgnon. However, subpixel size variations of the canopy remained difficult to track and

affected especially the comparison with the smaller footprint of FloX and RoX on the ground. Thus, it is advisable to examine the heterogeneity of the investigated canopy carefully with the best spatial resolution and visually explore the site when installing field spectrometers on the ground. The footprints of the ground measurements were chosen in order to be representative for a larger area with respect to the S-2 pixel-size and to minimize uncertainties related to spatial heterogeneity in this study. In both, OHP and Torgnon was the spatial location of ground measurements correctly recognized within one cluster of similar pixels. The ground measured temporal signatures overlapped with the temporal signatures associated with the corresponding cluster especially well during summer. In consequence, spatial clustering of S-2 pixels with respect to the associated temporal signatures in NDVI is considered a very useful tool to identify similar areas and to extrapolate the high-resolution temporal ground measurements, given that homogeneity of the canopy and representativeness of ground measurements can be assumed (Bador et al., 2015; Duveiller and Cescatti, 2016). However, care must be taken to account for the seasonality of the discrepancy between ground and satellite with respect to the temporal dynamics of the investigated ecosystem. Hence, extrapolation of information from the field spectrometer readings was not valid for times when the temporal signatures did not overlap well with the associated cluster and absolute temporal residuals were high. Likewise, the variability inside the pixel-associated clusters showed a seasonal pattern and can help to indicate the uncertainties around similar satellite pixels providing abundant ground coverage (Nagai et al., 2020). Uncertainties of field spectrometer readings are affected by morphological diversity of the canopy (Singh et al., 2015) and represent a challenge when generalizing insights into larger areas from the satellite. Thus, valid spatial extrapolation of high-resolution, temporal measurements into a larger area requires the assessment of the spatial uncertainty budget (Wen et al., 2020).

4.3. *Cloud filtering*

The automated field spectrometer systems FloX and RoX are capable of continuously monitoring one ROI at very high temporal and very high spectral resolution (Drolet et al., 2014). In contrast, atmospherically corrected S-2 TOC data depict an entire spatial scene of many pixels at a coarser temporal and coarser multispectral resolution (Linkosalmi et al., 2022). Only the harmonization of cloud-free data from both platforms is possible. Thus, the validation of cloud-free pairs of S-2 overpasses and overlapping measurements on ground was an important pre-requisite for this work. Therefore, an approach for cloud-filtering based on continuous down-welling radiance measured by automated field spectrometers on the ground was employed. The ground-based filtering approach outperformed the S-2 cloud masks and identified also small obstructions from high, thin and small clouds reliably in the limited areas around the spectrometer site. In contrast, using a cloud-mask and setting a threshold of zero for the percentage of cloud-coverage would not suffice to rule out small clouds inside the scene (Baetens et al., 2019). In consequence, total rejection of all data with non-zero cloud-cover was not feasible based on cloud-masks. Consequently, using ground-based down-welling radiance allowed for a much more selective filtering by rejecting data, which was actually affected by clouds at the time of the S-2 overpass at the spectrometer site. Since the hemispherical cosine diffusor of the FloX/RoX monitored rapid changes in irradiance continuously (Burkart et al., 2022), clouds and cloud shadows were identified precisely by measuring the discrepancy from a linear evolution of down-welling radiance for very short time windows, e.g. 20 min around the S-2 overpass. Cloud filtering using continuous ground measurements of irradiance is recommended only for experiments of limited spatial expanse around the spectrometer site, not exceeding the direct line of sight of the ground-based optics. The correct identification of clouds in satellite data remains challenging under rapidly changing atmospheric conditions to this day (Linkosalmi et al., 2022; Schläpfer et al., 2020b). Thus, cloud detection should be informed by the use of automated ground measurements when possible.

5. Conclusion

A network of standardized, automated field spectrometer systems was validated using Sentinel-2 TOC reflectance as reference in 10 different sites around the globe. Good overall agreement between field spectrometers and Sentinel-2 level 2-A TOC reflectance suggested mostly consistent reflectance data throughout the network. Deviations of individual samples and sites were mainly caused by slight spatial misalignments of Sentinel-2 pixels and the spectrometer footprints, by the instrument setup, atmospheric compensation and variable landscape heterogeneity. Future works should aim at correcting data product deviations from multiple ground sites using Sentinel-2 as a reference and move towards fully harmonized data. We observed a very good agreement between NDVI obtained from the field spectrometers and Sentinel-2, while the propagated errors from individual spectral bands were more noticeable with the more complex TCARI and EVI. The seasonal patterns of NDVI residuals on ground with respect to the satellite demonstrated increased uncertainties from summer to winter for the dynamic, heterogenous alpine ecosystem due to diverse vegetation phenology, snowfall and snowmelt, in contrast to a random distribution of residuals in a snow-free and homogenous oak forest in southern France. Thus, it is recommend to carefully consider the seasonal landscape dynamics when validating continuous ground measurements against satellite data. Furthermore, cloud filtering based on ground-measured irradiance showed a very robust way to eliminate overcast scenes in limited areas and outperformed conventional cloud-mask. We recommend to further exploit the potential for improving cloud-filtering of satellite data based on automated, continuous spectrometer measurements on the ground.

Validating the network of automated field spectrometers around the globe against Sentinel-2 demonstrated the potential of harmonizing standardized, hyperspectral, temporally dense reflectance data with respect to the satellite. The spatial domain of the satellite scale informed the assessment of uncertainties and assumptions of homogenous areas on the ground. Future works combining different optical sensors in various locations will benefit from harmonizing their data against Sentinel-2 as a vigorously standardized refence offering global coverage.

CRediT authorship contribution statement

Paul Naethe: Conceptualization, Methodology, Resources, Software, Validation, Visualization, Writing – original draft, Writing – review & editing. **Andrea De Sanctis:** Data curation, Formal analysis, Methodology, Software, Visualization. **Andreas Burkart:** Data curation, Funding acquisition, Writing – review & editing. **Petya K.E. Campbell:** Data curation, Resources, Writing – review & editing. **Roberto Colombo:** Data curation, Resources, Writing – review & editing. **Biagio Di Mauro:** Data curation, Resources, Writing – review & editing. **Alexander Damm:** Data curation, Resources, Writing – review & editing. **Tarek El-Madany:** Data curation, Resources. **Francesco Fava:** Data curation. **John A. Gamon:** Data curation, Resources, Writing – review & editing. **Karl F. Huemmrich:** Data curation, Resources, Writing – review & editing. **Mirco Migliavacca:** Data curation, Resources. **Eugenie Paul-Limoges:** Data curation, Resources, Writing – review & editing. **Uwe Rascher:** Conceptualization, Data curation, Resources, Writing – review & editing. **Micol Rossini:** Data curation, Resources, Writing – review & editing. **Dirk Schüttemeyer:** Data curation, Funding acquisition, Resources. **Giulia Tagliabue:** Data curation, Resources. **Yongguang Zhang:** Data curation, Resources, Writing – review & editing. **Tommaso Julitta:** Conceptualization, Funding acquisition, Project administration, Software, Supervision, Visualization, Writing – review & editing.

Declaration of competing interest

The authors declare that they have no known competing financial interests or personal relationships that could have appeared to influence the work reported in this paper.

Data availability

Data will be made available on request.

Acknowledgement

This work was supported in partsthrough CA17134 SENSECO (Optical synergies for spatiotemporal sensing of scalable ecophysiological traits) funded by COST (European Cooperation in Science and Technology, www.cost.eu).

References

Aasen, H., Bolten, A., 2018. Multi-temporal high-resolution imaging spectroscopy with hyperspectral 2D imagers – from theory to application. Remote Sens. Environ. 205, 374–389. https://doi.org/10.1016/j.rse.2017.10.043.

Acebron, K., Matsubara, S., Jedmowski, C., Emin, D., Muller, O., Rascher, U., 2021. Diurnal dynamics of nonphotochemical quenching in Arabidopsis npq mutants assessed by solar-induced fluorescence and reflectance measurements in the field. New Phytol. 229, 2104–2119. https://doi.org/10.1111/nph.16984.

Adler-Golden, S.M., Matthew, M.W., Anderson, G.P., Felde, G.W., Gardner, J.A., 2002. Algorithm for de-shadowing spectral imagery, p. 203. https://doi.org/10.1117/12.451691.

Aghabozorgi, S., Seyed Shirkhorshidi, A., Ying Wah, T., 2015. Time-series clustering – a decade review. Inf. Syst. 53, 16–38. https://doi.org/10.1016/j.is.2015.04.007.

Alberton, B., da Torres, R.S., Cancian, L.F., Borges, B.D., Almeida, J., Mariano, G.C., dos Santos, J., Morellato, L.P.C., 2017. Introducing digital cameras to monitor plant phenology in the tropics: applications for conservation. Perspect. Ecol. Conserv. 15, 82–90. https://doi.org/10.1016/J.PECON.2017.06.004.

Ariza, A., Robredo Irizar, M., Bayer, S., 2018. Empirical line model for the atmospheric correction of sentinel-2A MSI images in the Caribbean Islands. Eur. J. Remote Sens. 51, 765–776. https://doi.org/10.1080/22797254.2018.1482732.

Bador, M., Naveau, P., Gilleland, E., Castellà, M., Arivelo, T., 2015. Spatial clustering of summer temperature maxima from the CNRM-CM5 climate model ensembles & E-OBS over Europe. Weather Clim. Extrem. 9, 17–24. https://doi.org/10.1016/j.wace.2015.05.003.

Baetens, L., Desjardins, C., Hagolle, O., 2019. Validation of copernicus Sentinel-2 cloud masks obtained from MAJA, Sen2Cor, and FMask processors using reference cloud masks generated with a supervised active learning procedure. Remote Sens. 11, 433. https://doi.org/10.3390/rs11040433.

Ball, C.P., Marks, A.A., Green, P.D., MacArthur, A., Maturilli, M., Fox, N.P., King, M.D., 2015. Hemispherical-directional reflectance (HDRF) of windblown snow-covered Arctic tundra at large solar zenith angles. IEEE Trans. Geosci. Remote Sens. 53, 5377–5387. https://doi.org/10.1109/TGRS.2015.2421733.

Bioucas-Dias, J.M., Plaza, A., Camps-Valls, G., Scheunders, P., Nasrabadi, N., Chanussot, J., 2013. Hyperspectral remote sensing data analysis and future challenges. IEEE Geosci. Remote Sens. Mag. 1, 6–36. https://doi.org/10.1109/MGRS.2013.2244672.

Biriukova, K., Celesti, M., Evdokimov, A., Pacheco-Labrador, J., Julitta, T., Migliavacca, M., Giardino, C., Miglietta, F., Colombo, R., Panigada, C., Rossini, M., 2020. Effects of varying solar-view geometry and canopy structure on solar-induced chlorophyll fluorescence and PRI. Int. J. Appl. Earth Obs. Geoinf. 89, 102069 https://doi.org/10.1016/j.jag.2020.102069.

Buman, B., Hueni, A., Colombo, R., Cogliati, S., Celesti, M., Julitta, T., Burkart, A., Siegmann, B., Rascher, U., Drusch, M., Damm, A., 2022. Towards consistent assessments of in situ radiometric measurements for the validation of fluorescence satellite missions. Remote Sens. Environ. 274 https://doi.org/10.1016/j.rse.2022.112984.

Burkart, A., Aasen, H., Alonso, L., Menz, G., Bareth, G., Rascher, U., 2015a. Angular dependency of hyperspectral measurements over wheat characterized by a novel UAV based goniometer. Remote Sens. 7, 725–746. https://doi.org/10.3390/rs70100725.

Burkart, A., Schickling, A., Mateo, M.P.C., Wrobel, T.J., Rossini, M., Cogliati, S., Julitta, T., Rascher, U., 2015b. A method for uncertainty assessment of passive sun-induced chlorophyll fluorescence retrieval using an infrared reference light. IEEE Sensors J. 15 https://doi.org/10.1109/JSEN.2015.2422894.

Burkart, A., Kennedy, M., Näthe, P., Julitta, T., 2022. Iterative design of a high light throughput cosine receptor fore optic for unattended proximal remote sensing. SPIE J. Appl. Remote Sens. 16, 1–9. https://doi.org/10.1117/1.JRS.16.044513.

Caballero, I., Fernández, R., Escalante, O.M., Mamán, L., Navarro, G., 2020. New capabilities of sentinel-2A/B satellites combined with in situ data for monitoring small harmful algal blooms in complex coastal waters. Sci. Rep. 10, 1–14. https://doi.org/10.1038/s41598-020-65600-1.

Campbell, P., Huemmrich, K., Middleton, E., Ward, L., Julitta, T., Daughtry, C., Burkart, A., Russ, A., Kustas, W., 2019. Diurnal and seasonal variations in chlorophyll fluorescence associated with photosynthesis at leaf and canopy scales. Remote Sens. 11, 488. https://doi.org/10.3390/rs11050488.

Castro-Esau, K.L., Sánchez-Azofeifa, G.A., Rivard, B., 2006. Comparison of spectral indices obtained using multiple spectroradiometers. Remote Sens. Environ. 103, 276–288. https://doi.org/10.1016/j.rse.2005.01.019.

Cavender-Bares, J., Gamon, J.A., Townsend, P.A., 2020. Remote Sensing of Plant Biodiversity. Springer Open. https://doi.org/10.1007/978-3-030-33157-3.

Chang, C.Y.-Y., Wen, J., Han, J., Kira, O., Levonne, J., Melkonian, J., Riha, S.J., Skovira, J., Ng, S., Gu, L., Wood, J.D., Näthe, P., Sun, Y., 2021. Unpacking the drivers of diurnal dynamics of sun-induced chlorophyll fluorescence (SIF): canopy structure, plant physiology, instrument configuration and retrieval methods. Remote Sens. Environ. 265, 112672 https://doi.org/10.1016/j.rse.2021.112672.

Cheng, Y., Gamon, J.A., Fuentes, D.A., Mao, Z., Sims, D.A., Qiu, H. Lie, Claudio, H., Huete, A., Rahman, A.F., 2006. A multi-scale analysis of dynamic optical signals in a Southern California chaparral ecosystem: a comparison of field, AVIRIS and MODIS data. Remote Sens. Environ. 103, 369–378. https://doi.org/10.1016/j.rse.2005.06.013.

Cogliati, S., Rossini, M., Julitta, T., Meroni, M., Schickling, A., Burkart, A., Pinto, F., Rascher, U., Colombo, R., 2015. Continuous and long-term measurements of reflectance and sun-induced chlorophyll fluorescence by using novel automated field spectroscopy systems. Remote Sens. Environ. 164, 270–281. https://doi.org/10.1016/j.rse.2015.03.027.

Damm, A., Guanter, L., Verhoef, W., Schläpfer, D., Garbari, S., Schaepman, M.E., 2015. Impact of varying irradiance on vegetation indices and chlorophyll fluorescence derived from spectroscopy data. Remote Sens. Environ. https://doi.org/10.1016/j.rse.2014.09.031.

Debella-Gilo, M., Gjertsen, A.K., 2021. Mapping seasonal agricultural land use types using deep learning on Sentinel-2 image time series. Remote Sens. 13, 289. https://doi.org/10.3390/rs13020289.

Dechant, B., Ryu, Y., Badgley, G., Köhler, P., Rascher, U., Migliavacca, M., Zhang, Y., Tagliabue, G., Guan, K., Rossini, M., Goulas, Y., Zeng, Y., Frankenberg, C., Berry, J. A., 2022. NIRVP: a robust structural proxy for sun-induced chlorophyll fluorescence and photosynthesis across scales. Remote Sens. Environ. 268, 112763 https://doi.org/10.1016/j.rse.2021.112763.

Drolet, G., Wade, T., Nichol, C.J., MacLellan, C., Levula, J., Porcar-Castell, A., Nikinmaa, E., Vesala, T., 2014. A temperature-controlled spectrometer system for continuous and unattended measurements of canopy spectral radiance and reflectance. Int. J. Remote Sens. 35, 1769–1785. https://doi.org/10.1080/01431161.2014.882035.

Drusch, M., Del Bello, U., Carlier, S., Colin, O., Fernandez, V., Gascon, F., Hoersch, B., Isola, C., Laberinti, P., Martimort, P., Meygret, A., Spoto, F., Sy, O., Marchese, F., Bargellini, P., 2012. Sentinel-2: ESA's optical high-resolution mission for GMES operational services. Remote Sens. Environ. 120, 25–36. https://doi.org/10.1016/j.rse.2011.11.026.

Duveiller, G., Cescatti, A., 2016. Spatially downscaling sun-induced chlorophyll fluorescence leads to an improved temporal correlation with gross primary productivity. Remote Sens. Environ. 182, 72–89. https://doi.org/10.1016/j.rse.2016.04.027.

Eitel, J.U.H., Keefe, R.F., Long, D.S., Davis, A.S., Vierling, L.A., 2010. Active ground optical remote sensing for improved monitoring of seedling stress in nurseries. Sensors 10, 2843–2850. https://doi.org/10.3390/s100402843.

ESRI, 2021. World Imagery [basemap]. Scale not given. [WWW Document]. World Imag. URL. https://www.arcgis.com/home/item.html?id=10df2279f9684e4a9f6a7f08febac2a9 (accessed 1.12.23).

Etzold, S., Sterck, F., Bose, A.K., Braun, S., Buchmann, N., Eugster, W., Gessler, A., Kahmen, A., Peters, R.L., Vitasse, Y., Walthert, L., Ziemińska, K., Zweifel, R., 2022. Number of growth days and not length of the growth period determines radial stem growth of temperate trees. Ecol. Lett. 25, 427–439. https://doi.org/10.1111/ele.13933.

Fu, Y., Zhang, H., Dong, W., Yuan, W., 2014. Comparison of phenology models for predicting the onset of growing season over the northern hemisphere. PLoS One 9. https://doi.org/10.1371/journal.pone.0109544.

Gamon, J.A., 2015. Reviews and syntheses: optical sampling of the flux tower footprint. Biogeosciences. https://doi.org/10.5194/bg-12-4509-2015.

Gamon, J.A., Peñuelas, J., Field, C.B., 1992. A narrow-waveband spectral index that tracks diurnal changes in photosynthetic efficiency. Remote Sens. Environ. https://doi.org/10.1016/0034-4257(92)90059-S.

Gamon, J.A., Field, C.B., Hartley, A.E., Joel, G., Penuelas, J., Riccardo Valentini, A., 1995. Relationships between NDVI, canopy structure, and photosynthesis in three Californian vegetation types. Ecol. Appl. 5, 28–41.

Gamon, J.A., Rahman, A.F., Dungan, J.L., Schildhauer, M., Huemmrich, K.F., 2006. Spectral network (SpecNet)—what is it and why do we need it? Remote Sens. Environ. 103, 227–235. https://doi.org/10.1016/j.rse.2006.04.003.

Gamon, J.A., Coburn, C., Flanagan, L.B., Huemmrich, K.F., Kiddle, C., Sanchez-Azofeifa, G.A., Thayer, D.R., Vescovo, L., Gianelle, D., Sims, D.A., Rahman, A.F., Pastorello, G.Z., 2010. SpecNet revisited: bridging flux and remote sensing communities. Can. J. Remote. Sens. 36, S376–S390. https://doi.org/10.5589/m10-067.

Gamon, J.A., Kovalchuck, O., Wong, C.Y.S., Harris, A., Garrity, S.R., 2015. Monitoring seasonal and diurnal changes in photosynthetic pigments with automated PRI and NDVI sensors. Biogeosciences 12. https://doi.org/10.5194/bg-12-4149-2015.

Gielen, B., Op de Beek, M., Loustau, D., Ceulemans, R., Jordan, A., Papale, D., 2017. Integrated Carbon Observation System (ICOS). In: Chabbi, A., Loescher, H.W. (Eds.),

Terrestrial Ecosystem Research Infrastructures. CRC Press, Boca Raton, FL. https://doi.org/10.1201/9781315368252, 2017.
Gorelick, N., Hancher, M., Dixon, M., Ilyushchenko, S., Thau, D., Moore, R., 2017. Google earth engine: planetary-scale geospatial analysis for everyone. Remote Sens. Environ. 202, 18–27. https://doi.org/10.1016/j.rse.2017.06.031.
Haboudane, D., Miller, J.R., Tremblay, N., Zarco-Tejada, P.J., Dextraze, L., 2002. Integrated narrow-band vegetation indices for prediction of crop chlorophyll content for application to precision agriculture. Remote Sens. Environ. 81, 416–426.
Hank, T.B., Berger, K., Bach, H., Clevers, J.G.P.W., Gitelson, A., Zarco-Tejada, P., Mauser, W., 2018. Spaceborne imaging spectroscopy for sustainable agriculture: contributions and challenges. Surv. Geophys. https://doi.org/10.1007/s10712-018-9492-0.
Herrmann, I., Karnieli, A., Bonfil, D.J., Cohen, Y., Alchanatis, V., 2010. SWIR-based spectral indices for assessing nitrogen content in potato fields. Int. J. Remote Sens. 31, 5127–5143. https://doi.org/10.1080/01431160903283892.
Honkavaara, E., Khoramshahi, E., 2018. Radiometric correction of close-range spectral image blocks captured using an unmanned aerial vehicle with a radiometric block adjustment. Remote Sens. 10, 256. https://doi.org/10.3390/rs10020256.
Hueni, A., Damm, A., Kneubuehler, M., Schlapfer, D., Schaepman, M.E., 2017. Field and airborne spectroscopy cross validation -some considerations. IEEE J. Sel. Top. Appl. Earth Obs. Remote Sens. 10, 1117–1135. https://doi.org/10.1109/JSTARS.2016.2593984.
Jiang, Z., Huete, A.R., Chen, J., Chen, Y., Li, J., Yan, G., Zhang, X., 2006. Analysis of NDVI and scaled difference vegetation index retrievals of vegetation fraction. Remote Sens. Environ. 101, 366–378. https://doi.org/10.1016/j.rse.2006.01.003.
Julitta, T., Corp, L.A., Rossini, M., Burkart, A., Cogliati, S., Davies, N., Hom, M., Mac Arthur, A., Middleton, E.M., Rascher, U., Schickling, A., Colombo, R., 2016. Comparison of sun-induced chlorophyll fluorescence estimates obtained from four portable field spectroradiometers. Remote Sens. 8 https://doi.org/10.3390/rs8020122.
Kanniah, K.D., Beringer, J., North, P., Hutley, L., 2012. Control of atmospheric particles on diffuse radiation and terrestrial plant productivity: a review. Prog. Phys. Geogr. https://doi.org/10.1177/0309133311434244.
Kaskaoutis, D.G., Kambezidis, H.D., Kumar Kharol, S., Badarinath, K.V.S., 2008. The diffuse-to-global spectral irradiance ratio as a cloud-screening technique for radiometric data. J. Atmos. Solar-Terrestrial Phys. https://doi.org/10.1016/j.jastp.2008.04.013.
Kokhanovsky, A., Di Mauro, B., Garzonio, R., Colombo, R., 2021. Retrieval of dust properties from spectral snow reflectance measurements. Front. Environ. Sci. 9 https://doi.org/10.3389/fenvs.2021.644551.
Krämer, J., Siegmann, B., Kraska, T., Muller, O., Rascher, U., 2021. The potential of spatial aggregation to extract remotely sensed sun-induced fluorescence (SIF) of small-sized experimental plots for applications in crop phenotyping. Int. J. Appl. Earth Obs. Geoinf. 104, 102565 https://doi.org/10.1016/j.jag.2021.102565.
Lama, G.F.C., Crimaldi, M., De Vivo, A., Chirico, G.B., Sarghini, F., 2021a. Eco-hydrodynamic characterization of vegetated flows derived by UAV-based imagery. In: 2021 IEEE International Workshop on Metrology for Agriculture and Forestry (MetroAgriFor), pp. 273–278. https://doi.org/10.1109/MetroAgriFor52389.2021.9628749.
Lama, G.F.C., Rillo Migliorini Giovannini, M., Errico, A., Mirzaei, S., Chirico, G.B., Preti, F., 2021b. The impacts of Nature Based Solutions (NBS) on vegetated flows' dynamics in urban areas. In: 2021 IEEE International Workshop on Metrology for Agriculture and Forestry (MetroAgriFor), pp. 58–63. https://doi.org/10.1109/MetroAgriFor52389.2021.9628438.
Lense, G.H.E., Lämmle, L., Ayer, J.E.B., Lama, G.F.C., Rubira, F.G., Mincato, R.L., 2023. Modeling of soil loss by water erosion and its impacts on the Cantareira System, Brazil. Water (Switzerland) 15. https://doi.org/10.3390/w15081490.
Li, Y., Chen, J., Ma, Q., Zhang, H.K., Liu, J., 2018. Evaluation of sentinel-2A surface reflectance derived using Sen2Cor in North America. IEEE J. Sel. Top. Appl. Earth Obs. Remote Sens. 11, 1997–2021. https://doi.org/10.1109/JSTARS.2018.2835823.
Linkosalmi, M., Tuovinen, J.-P., Nevalainen, O., Peltoniemi, M., Taniş, C.M., Arslan, A. N., Rainne, J., Lohila, A., Laurila, T., Aurela, M., 2022. Tracking vegetation phenology of pristine northern boreal peatlands by combining digital photography with CO2 flux and remote sensing data. Biogeosciences Discuss. Prepr. https://doi.org/10.5194/bg-2022-58.
Liu, H.Q., Huete, A., 1995. A feedback based modification of the NDVI to minimize canopy background and atmospheric noise. IEEE Trans. Geosci. Remote Sens. 33, 457–465. https://doi.org/10.1109/tgrs.1995.8746027.
Liu, X., Hou, Z., Shi, Z., Bo, Y., Cheng, J., 2017. A shadow identification method using vegetation indices derived from hyperspectral data. Int. J. Remote Sens. 38, 5357–5373. https://doi.org/10.1080/01431161.2017.1338785.
Ma, X., Mahecha, M.D., Migliavacca, M., van der Plas, F., Benavides, R., Ratcliffe, S., Kattge, J., Richter, R., Musavi, T., Baeten, L., Barnoaiea, I., Bohn, F.J., Bouriaud, O., Bussotti, F., Coppi, A., Domisch, T., Huth, A., Jaroszewicz, B., Joswig, J., Pabon-Moreno, D.E., Papale, D., Selvi, F., Laurin, G.V., Valladares, F., Reichstein, M., Wirth, C., 2019. Inferring plant functional diversity from space: the potential of Sentinel-2. Remote Sens. Environ. 233, 111368 https://doi.org/10.1016/j.rse.2019.111368.
Ma, H., Liang, S., Xiong, C., Wang, Q., Jia, A., Li, B., 2022. Global land surface 250 m 8 d fraction of absorbed photosynthetically active radiation (FAPAR) product from 2000 to 2021. Earth Syst. Sci. Data 14, 5333–5347. https://doi.org/10.5194/essd-14-5333-2022.
Main, R., Cho, M.A., Mathieu, R., O'Kennedy, M.M., Ramoelo, A., Koch, S., 2011. An investigation into robust spectral indices for leaf chlorophyll estimation. ISPRS J. Photogramm. Remote Sens. 66, 751–761. https://doi.org/10.1016/j.isprsjprs.2011.08.001.
Malenovský, Z., Ufer, C., Lhotáková, Z., Clevers, J.G.P.W., Schaepman, M.E., Albrechtová, J., Cudlín, P., 2006. A new hyperspectral index for chlorophyll estimation of a forest canopy: area under curve normalised to maximal band depth between 650-725 nm. EARSeL eProceedings.
Martini, D., Sakowska, K., Wohlfahrt, G., Pacheco-Labrador, J., van der Tol, C., Porcar-Castell, A., Magney, T.S., Carrara, A., Colombo, R., El-Madany, T.S., Gonzalez-Cascon, R., Martín, M.P., Julitta, T., Moreno, G., Rascher, U., Reichstein, M., Rossini, M., Migliavacca, M., 2022. Heatwave breaks down the linearity between sun-induced fluorescence and gross primary production. New Phytol. https://doi.org/10.1111/nph.17920.
Meroni, M., Barducci, A., Cogliati, S., Castagnoli, F., Rossini, M., Busetto, L., Migliavacca, M., Cremonese, E., Galvagno, M., Colombo, R., Di Cella, U.M., 2011. The hyperspectral irradiometer, a new instrument for long-term and unattended field spectroscopy measurements. Rev. Sci. Instrum. 82 https://doi.org/10.1063/1.3574360.
Metzger, S., Ayres, E., Durden, D., Florian, C., Lee, R., Lunch, C., Luo, H., Pingintha-Durden, N., Roberti, J.A., SanClements, M., Sturtevant, C., Xu, K., Zulueta, R.C., 2019. From neon field sites to data portal: a community resource for surface-atmosphere research comes online. Bull. Am. Meteorol. Soc. 100, 2305–2325. https://doi.org/10.1175/BAMS-D-17-0307.1.
Migliavacca, M., Perez-Priego, O., Rossini, M., El-Madany, T.S., Moreno, G., van der Tol, C., Rascher, U., Berninger, A., Bessenbacher, V., Burkart, A., Carrara, A., Fava, F., Guan, J.H., Hammer, T.W., Henkel, K., Juarez-Alcalde, E., Julitta, T., Kolle, O., Martín, M.P., Musavi, T., Pacheco-Labrador, J., Pérez-Burgueño, A., Wutzler, T., Zaehle, S., Reichstein, M., 2017. Plant functional traits and canopy structure control the relationship between photosynthetic CO2 uptake and far-red sun-induced fluorescence in a Mediterranean grassland under different nutrient availability. New Phytol. 214, 1078–1091. https://doi.org/10.1111/nph.14437.
Mihai, L., Arthur, A. Mac, Hueni, A., Robinson, I., Sporea, D., 2018. Optimized spectrometers characterization procedure for near ground support of ESA FLEX observations: part 1 spectral calibration and characterisation. Remote Sens. https://doi.org/10.3390/rs10020289.
Milton, E.J., Schaepman, M.E., Anderson, K., Fox, N., 2007. Progress in field spectroscopy. Remote Sens. Environ. 113, S92–S109. https://doi.org/10.1016/j.rse.2007.08.001.
Mohammad, L., Bandyopadhyay, J., Sk, R., Mondal, I., Nguyen, T.T., Lama, G.F.C., Anh, D.T., 2023. Estimation of agricultural burned affected area using NDVI and dNBR satellite-based empirical models. J. Environ. Manag. 343, 118226 https://doi.org/10.1016/j.jenvman.2023.118226.
Mohammed, G.H., Colombo, R., Middleton, E.M., Rascher, U., van der Tol, C., Nedbal, L., Goulas, Y., Pérez-Priego, O., Damm, A., Meroni, M., Joiner, J., Cogliati, S., Verhoef, W., Malenovský, Z., Gastellu-Etchegorry, J.P., Miller, J.R., Guanter, L., Moreno, J., Moya, I., Berry, J.A., Frankenberg, C., Zarco-Tejada, P.J., 2019. Remote sensing of solar-induced chlorophyll fluorescence (SIF) in vegetation: 50 years of progress. Remote Sens. Environ. 231 https://doi.org/10.1016/j.rse.2019.04.030.
Naethe, P., Delaney, M., Julitta, T., 2020. Changes of NOx in urban air detected with monitoring VIS-NIR field spectrometer during the coronavirus pandemic: a case study in Germany. Sci. Total Environ. 748, 141286 https://doi.org/10.1016/j.scitotenv.2020.141286.
Naethe, P., Asgari, M., Kneer, C., Knieps, M., Jenal, A., Weber, I., Moelter, T., Dzunic, F., Deffert, P., Rommel, E., Delaney, M., Baschek, B., Rock, G., Bongartz, J., Burkart, A., 2023. Calibration and validation from ground to airborne and satellite level: joint application of time-synchronous field spectroscopy, drone, aircraft and Sentinel-2 imaging. PFG – J. Photogramm. Remote Sens. Geoinf. Sci. https://doi.org/10.1007/s41064-022-00231-x.
Nagai, S., Nasahara, K.N., Akitsu, T.K., Saitoh, T.M., Muraoka, H., 2020. Importance of the collection of abundant ground-truth data for accurate detection of spatial and temporal variability of vegetation by satellite remote sensing. Biogeochem. Cycles Ecol. Drivers Environ. Impact. wiley 223–244. https://doi.org/10.1002/9781119413332.ch11.
Norton, A.J., Rayner, P.J., Koffi, E.N., Scholze, M., Silver, J.D., Wang, Y.-P., 2019. Estimating global gross primary productivity using chlorophyll fluorescence and a data assimilation system with the BETHY-SCOPE model. Biogeosci. Discuss. 1–45 https://doi.org/10.5194/bg-2019-83.
Olsson, P.-O., Vivekar, A., Adler, K., Garcia Millan, V.E., Koc, A., Alamrani, M., Eklundh, L., 2021. Radiometric correction of multispectral UAS images: evaluating the accuracy of the parrot Sequoia camera and sunshine sensor. Remote Sens. 13, 577. https://doi.org/10.3390/rs13040577.
Oxoli, D., Brovelli, M.A., Frizzi, D., Martinati, S., 2020. Detection of land cover displacements through time-series analysis of multispectral satellite imagery: application to desert. In: International Archives of the Photogrammetry, Remote Sensing and Spatial Information Sciences - ISPRS Archives. International Society for Photogrammetry and Remote Sensing, pp. 739–744. https://doi.org/10.5194/isprs-archives-XLIII-B3-2020-739-2020.
Painter, T.H., Dozier, J., 2004. Measurements of the hemispherical-directional reflectance of snow at fine spectral and angular resolution. J. Geophys. Res. Atmos. 109 https://doi.org/10.1029/2003JD004458.
Peano, D., Hemming, D., Materia, S., Delire, C., Fan, Y., Joetzjer, E., Lee, H., Nabel, J.E. M.S., Park, T., Peylin, P., Wärlind, D., Wiltshire, A., Zaehle, S., 2021. Plant phenology evaluation of CRESCENDO land surface models-Part 1: Start and end of the growing season. Biogeosciences 18, 2405–2428. https://doi.org/10.5194/bg-18-2405-2021.
Pérez-Harguindeguy, N., Díaz, S., Garnier, E., Lavorel, S., Poorter, H., Jaureguiberry, P., Bret-Harte, M.S., Cornwell, W.K., Craine, J.M., Gurvich, D.E., Urcelay, C., Veneklaas, E.J., Reich, P.B., Poorter, L., Wright, I.J., Ray, P., Enrico, L., Pausas, J.G., De Vos, A.C., Buchmann, N., Funes, G., Quétier, F., Hodgson, J.G., Thompson, K.,

Morgan, H.D., Ter Steege, H., Van Der Heijden, M.G.A., Sack, L., Blonder, B., Poschlod, P., Vaieretti, M.V., Conti, G., Staver, A.C., Aquino, S., Cornelissen, J.H.C., 2013. New handbook for standardised measurement of plant functional traits worldwide. Aust. J. Bot. https://doi.org/10.1071/BT12225.

Petitjean, F., Weber, J., 2014. Efficient satellite image time series analysis under time warping. IEEE Geosci. Remote Sens. Lett. 11, 1143–1147. https://doi.org/10.1109/LGRS.2013.2288358.

Picard, G., Libois, Q., Arnaud, L., Verin, G., Dumont, M., 2016. Development and calibration of an automatic spectral albedometer to estimate near-surface snow SSA time series. Cryosphere 10, 1297–1316. https://doi.org/10.5194/tc-10-1297-2016.

Picard, G., Dumont, M., Lamare, M., Tuzet, F., Larue, F., Pirazzini, R., Arnaud, L., 2020. Spectral albedo measurements over snow-covered slopes: theory and slope effect corrections. Cryosphere 14, 1497–1517. https://doi.org/10.5194/tc-14-1497-2020.

Pieruschka, R., Albrecht, H., Muller, O., Berry, J.A., Klimov, D., Kolber, Z.S., Malenovský, Z., Rascher, U., 2014. Daily and seasonal dynamics of remotely sensed photosynthetic efficiency in tree canopies. Mol. Hum. Reprod. 34 https://doi.org/10.1093/treephys/tpu035.

Pirone, D., Cimorelli, L., Del Giudice, G., Pianese, D., 2023. Short-term rainfall forecasting using cumulative precipitation fields from station data: a probabilistic machine learning approach. J. Hydrol. 617, 128949 https://doi.org/10.1016/j.jhydrol.2022.128949.

Porcar-Castell, A., Mac Arthur, A., Rossini, M., Eklundh, L., Pacheco-Labrador, J., Anderson, K., Balzarolo, M., Martín, M.P., Jin, H., Tomelleri, E., Cerasoli, S., Sakowska, K., Hueni, A., Julitta, T., Nichol, C.J., Vescovo, L., 2015. EUROSPEC: at the interface between remote-sensing and ecosystem CO2flux measurements in Europe. Biogeosciences 12, 6103–6124. https://doi.org/10.5194/bg-12-6103-2015.

R Core Team, 2017. R: A Language and Environment for Statistical Computing. R Foundation for Statistical Computing, Vienna, Austria.

Rejichi, S., Chaabane, F., 2015. Satellite image time series classification and analysis using an adapted graph labeling. In: 2015 8th International Workshop on the Analysis of Multitemporal Remote Sensing Images, Multi-Temp 2015. Institute of Electrical and Electronics Engineers Inc. https://doi.org/10.1109/Multi-Temp.2015.7245747

Rossini, M., Meroni, M., Migliavacca, M., Manca, G., Cogliati, S., Busetto, L., Picchi, V., Cescatti, A., Seufert, G., Colombo, R., 2010. High resolution field spectroscopy measurements for estimating gross ecosystem production in a rice field. Agric. For. Meteorol. 150, 1283–1296. https://doi.org/10.1016/j.agrformet.2010.05.011.

Schaepman, M.E., Dangel, S., 2000. Solid laboratory calibration of a nonimaging spectroradiometer. Appl. Opt. 39, 3754–3764. https://doi.org/10.1364/AO.39.003754.

Schläpfer, D., Popp, C., Richter, R., 2020a. Drone data atmospheric correction concept for multi-and hyperspectral imagery-the droacor model. In: International Archives of the Photogrammetry, Remote Sensing and Spatial Information Sciences - ISPRS Archives. International Society for Photogrammetry and Remote Sensing, pp. 473–478. https://doi.org/10.5194/isprs-archives-XLIII-B3-2020-473-2020.

Schläpfer, D., Richter, R., Reinartz, P., 2020b. Elevation-dependent removal of cirrus clouds in satellite imagery. Remote Sens. 12 https://doi.org/10.3390/rs12030494.

Schmitt, M., Zhu, X.X., 2016. Data Fusion and Remote Sensing: An ever-growing relationship. IEEE Geosci. Remote Sens. Mag. https://doi.org/10.1109/MGRS.2016.2561021.

Sefrin, O., Riese, F.M., Keller, S., 2021. Deep learning for land cover change detection. Remote Sens. 13, 1–27. https://doi.org/10.3390/rs13010078.

Shahtahmassebi, A., Yang, N., Wang, K., Moore, N., Shen, Z., 2013. Review of shadow detection and de-shadowing methods in remote sensing. Chin. Geogr. Sci. 23, 403–420. https://doi.org/10.1007/s11769-013-0613-x.

Siegmann, B., Cendrero-Mateo, M.P., Cogliati, S., Damm, A., Gamon, J., Herrera, D., Jedmowski, C., Junker-Frohn, L.V., Kraska, T., Muller, O., Rademske, P., van der Tol, C., Quiros-Vargas, J., Yang, P., Rascher, U., 2021. Downscaling of far-red solar-induced chlorophyll fluorescence of different crops from canopy to leaf level using a diurnal data set acquired by the airborne imaging spectrometer HyPlant. Remote Sens. Environ. 264 https://doi.org/10.1016/j.rse.2021.112609.

Singh, A., Serbin, S.P., McNeil, B.E., Kingdon, C.C., Townsend, P.A., 2015. Imaging spectroscopy algorithms for mapping canopy foliar chemical and morphological traits and their uncertainties. Ecol. Appl. 25, 2180–2197. https://doi.org/10.1890/14-2098.1.

Stow, D., Nichol, C.J., Wade, T., Assmann, J.J., Simpson, G., Helfter, C., 2019. Illumination geometry and flying height influence surface reflectance and ndvi derived from multispectral UAS imagery. Drones 3, 1–28. https://doi.org/10.3390/drones3030055.

Tucker, C.J., 1979. Red and photographic infrared linear combinations for monitoring vegetation. Remote Sens. Environ. 8, 127–150. https://doi.org/10.1016/0034-4257(79)90013-0.

Vargas, J.Q., Bendig, J., Arthur, A. Mac, Burkart, A., Julitta, T., Maseyk, K., Thomas, R., Siegmann, B., Rossini, M., Celesti, M., Schüttemeyer, D., Kraska, T., Muller, O., Rascher, U., 2020. Unmanned aerial systems (UAS)-based methods for solar induced chlorophyll fluorescence (SIF) retrieval with non-imaging spectrometers: State of the art. Remote Sens. 12 https://doi.org/10.3390/rs12101624.

Vincini, M., Calegari, F., Casa, R., 2016. Sensitivity of leaf chlorophyll empirical estimators obtained at Sentinel-2 spectral resolution for different canopy structures. Precis. Agric. 17, 313–331. https://doi.org/10.1007/s11119-015-9424-7.

Vogtli, M., Schlapfer, D., Richter, R., Hueni, A., Schaepman, M.E., Kneubuhler, M., 2021. About the transferability of topographic correction methods from spaceborne to airborne optical data. IEEE J. Sel. Top. Appl. Earth Obs. Remote Sens. 14, 1348–1362. https://doi.org/10.1109/JSTARS.2020.3039327.

Wagner, A., Hilgert, S., Kattenborn, T., Fuchs, S., 2018. Proximal VIS-NIR Spectrometry to retrieve substance concentrations in surface waters using partial least squares modelling. Water Sci. Technol. Water Supply. https://doi.org/10.2166/ws.2018.177.

Wallace, C.S., Dale, M.B., 2005. Hierarchical clusters of vegetation types. Community Ecol. 6, 57–74. https://doi.org/10.1556/ComEc.6.2005.1.7.

Wang, B., Jia, K., Liang, S., Xie, X., Wei, X., Zhao, X., Yao, Y., Zhang, X., 2018. Assessment of Sentinel-2 MSI spectral band reflectances for estimating fractional vegetation cover. Remote Sens. 10 https://doi.org/10.3390/rs10121927.

Wang, R., Bowling, D.R., Gamon, J.A., Smith, K.R., Yu, R., Hmimina, G., Ueyama, M., Noormets, A., Kolb, T.E., Richardson, A.D., Bourque, C.P.A., Bracho, R., Blanken, P. D., Black, T.A., Arain, M.A., 2023a. Snow-corrected vegetation indices for improved gross primary productivity assessment in North American evergreen forests. Agric. For. Meteorol. 340, 109600 https://doi.org/10.1016/j.agrformet.2023.109600.

Wang, R., Springer, K.R., Gamon, J.A., 2023b. Confounding effects of snow cover on remotely sensed vegetation indices of evergreen and deciduous trees: an experimental study. Glob. Chang. Biol. https://doi.org/10.1111/gcb.16916.

Wemett, B.D., Riek, J.K., Leathers, R.A., 2009. Dynamic thresholding for hyperspectral shadow detection using Levenberg-Marquardt minimization on multiple Gaussian illumination distributions, 7334, 733411. https://doi.org/10.1117/12.817826.

Wen, J., Köhler, P., Duveiller, G., Parazoo, N.C., Magney, T.S., Hooker, G., Yu, L., Chang, C.Y., Sun, Y., 2020. A framework for harmonizing multiple satellite instruments to generate a long-term global high spatial-resolution solar-induced chlorophyll fluorescence (SIF). Remote Sens. Environ. 239 https://doi.org/10.1016/j.rse.2020.111644.

Yao, Xinfeng, Yao, Xia, Jia, W., Tian, Y., Ni, J., Cao, W., Zhu, Y., 2013. Comparison and intercalibration of vegetation indices from different sensors for monitoring above-ground plant nitrogen uptake in winter wheat. Sensors (Switzerland) 13, 3109–3130. https://doi.org/10.3390/s130303109.

Zagajewski, B., Tømmervik, H., Bjerke, J.W., Raczko, E., Bochenek, Z., Klos, A., Jarocińska, A., Lavender, S., Ziólkowski, D., 2017. Intraspecific differences in spectral reflectance curves as indicators of reduced vitality in high-arctic plants. Remote Sens. 9 https://doi.org/10.3390/rs9121289.